

Contradistinguisher: A Vapnik's Imperative to Unsupervised Domain Adaptation

Sourabh Balgi  and Ambedkar Dukkipati 

Abstract—A complex combination of simultaneous supervised-unsupervised learning is believed to be the key to humans performing tasks seamlessly across multiple domains or tasks. This phenomenon of cross-domain learning has been very well studied in domain adaptation literature. Recent domain adaptation works rely on an indirect way of first aligning the source and target domain distributions and then train a classifier on the labeled source domain to classify the target domain. However, this approach has the main drawback that obtaining a near-perfect alignment of the domains in itself might be difficult/impossible (e.g., language domains). To address this, we follow Vapnik's imperative of statistical learning that states any desired problem should be solved in the most direct way rather than solving a more general intermediate task and propose a direct approach to domain adaptation that does not require domain alignment. We propose a model referred Contradistinguisher that learns contrastive features and whose objective is to jointly learn to contradistinguish the unlabeled target domain in an unsupervised way and classify in a supervised way on the source domain. We achieve the state-of-the-art on Office-31 and VisDA-2017 datasets in both single-source and multi-source settings. We also demonstrate that the contradistinguish loss improves the model performance by increasing the shape bias.

Index Terms—Contrastive Feature Learning, Deep Learning, Domain Adaptation, Transfer Learning, Unsupervised Learning.

1 INTRODUCTION

THE recent success of deep neural networks for supervised learning tasks in several areas like computer vision, speech, natural language processing can be attributed to the models that are trained on large amounts of labeled data. However, acquiring massive amounts of labeled data in some domains can be very expensive or not possible at all. Additionally, the amount of time required for labeling the data to use existing deep learning techniques can be very high initially for a new domain. This is known as *cold-start*. On the contrary, cost-effective unlabeled data can be easily obtained in large amounts for most new domains. So, one can aim to transfer the knowledge from a labeled source domain to perform tasks on an unlabeled target domain. To study this, under the purview of transductive transfer learning, several approaches like domain adaptation, sample selection bias, co-variance shift have been explored in recent times.

Existing domain adaptation approaches mostly rely on domain alignment, i.e., align both domains so that they are superimposed and indistinguishable in the latent space. This domain alignment can be achieved in three main ways: (a) discrepancy-based methods [1], [2], [3], [4], [5], [6], [7], [8], [9], [10], [11], [12], [13], [14], (b) reconstruction-based methods [15], [16], and (c) adversarial adaptation methods [17], [18], [19], [20], [21], [22], [23], [24], [25], [26], [27], [28], [29], [30], [31], [32], [33], [34], [35].

These domain alignment strategies of indirectly addressing the task of unlabeled target domain classification have three main drawbacks. (i) The sub-task of obtaining a perfect

alignment of the domain in itself might be impossible or very difficult due to large domain shift (e.g., language domains). (ii) The use of multiple classifiers and/or GANs to align the distributions unnecessarily increases the complexity of the neural networks leading to over-fitting in many cases. (iii) Due to distribution alignment, the domain-specific information is lost as the domains get morphed.

A particular case where the domain alignment and the classifier trained on the source domain might fail is in the case that the target domain is more suited to classification task than the source domain which has lower classification performance. In this case, it is advised to perform the classification directly on the unlabeled target domain in an unsupervised manner as domain alignment onto less suited source domain only leads to loss of information. It is reasonable to assume that for the main objective of unlabeled target domain classification, one can use all the information in the target domain and optionally incorporate any useful information from the labeled source domain and not the other way around. These drawbacks push us to challenge the idea of solving domain adaptation problems without solving the general problem of domain alignment.

In this work, we study unsupervised domain adaptation by learning contrastive features in the unlabeled target domain in a fully unsupervised manner with the help of classifier simultaneously trained on the labeled source domain. More importantly, we derive our motivation from the **Vapnik's imperative** that motivated the statistical learning theory [36], [37].

"When solving a given problem, try to avoid solving a more general problem as an intermediate step." [37]

In the context of domain adaptation, the desired problem is classification on the unlabeled target domain and domain alignment followed by most standard methods is

- S. Balgi and A. Dukkipati (Contact Author) are with the Department of Computer Science and Automation, Indian Institute of Science, Bengaluru, Karnataka, India, 560012.
E-mail: {sourabhbaldi, ambedkar}@iisc.ac.in

the general intermediate. Considering the various drawback of domain alignment approach and based on Vapnik’s imperative, in this paper, we propose a method for domain adaptation that does not require domain alignment and approach the problem directly.

This work extends our earlier conference paper [38] in the following way. (i) We provide additional experimental results on more complex domain adaptation dataset Office-31 [39] which includes images from three different sources, AMAZON (\mathcal{A}), DSLR (\mathcal{D}), and WEBCAM (\mathcal{W}) categorized into three domains respectively with only few labeled high resolution images. (ii) We provide additional experimental results on the benchmark VisDA-2017 [40] dataset for unsupervised domain adaptation that includes synthetic and real-world images from 12 different classes. (iii) We provide several ablation studies and demonstrations that will provide insights into the working of our proposed method CUDA [38]. Additionally, we demonstrate that the proposed contradistinguish loss helps learning high-level features in the image related to the shapes of the objects. (iv) We extend our algorithm to the more complex case of multi-source domain adaptation and establish benchmark results on Office-31 [39] dataset.

A summary of our contributions in this paper are as follows.

- 1) We propose a simple method Contradistinguisher for Unsupervised Domain Adaptation (CUDA) that directly addresses the problem of domain adaptation by learning a single classifier, which we refer to as Contradistinguisher, jointly in an unsupervised manner over the unlabeled target domain and in a supervised manner over the labeled source domain. Hence, overcoming the drawbacks of distribution alignment based techniques.
- 2) We formulate a ‘contradistinguish loss’ to directly utilize unlabeled target domain and address the classification task using unsupervised feature learning. Note that a similar approach called DisCoder [41] was used for a much simpler task of semi-supervised feature learning on a single domain with no domain distribution shift.
- 3) We extend our experiments to more complex domain adaptation datasets Office-31 [39] and VisDA-2017 [40]. From our experiments, we show that by jointly training contradistinguisher on the source domain and the target domain distributions, we can achieve above/on-par results over several recently proposed domain adaptation methods.
- 4) We further demonstrate the simplicity and effectiveness of our proposed method by easily extending single-source domain adaptation to a more complex and general multi-source domain adaptation. We demonstrate the effectiveness of the multi-source domain adaptation extension by performing experiments on Office-31 [39] dataset in a multi-source setting.
- 5) Apart from these real-world benchmark datasets, we also validate the proposed method using the synthetically created toy-datasets. We use *scikit-learn* [42] to generate blobs (point clouds) with different source and target domain distribution shapes and orientations and perform simulation of our proposed method. These experiment are significant to confirm that CUDA works

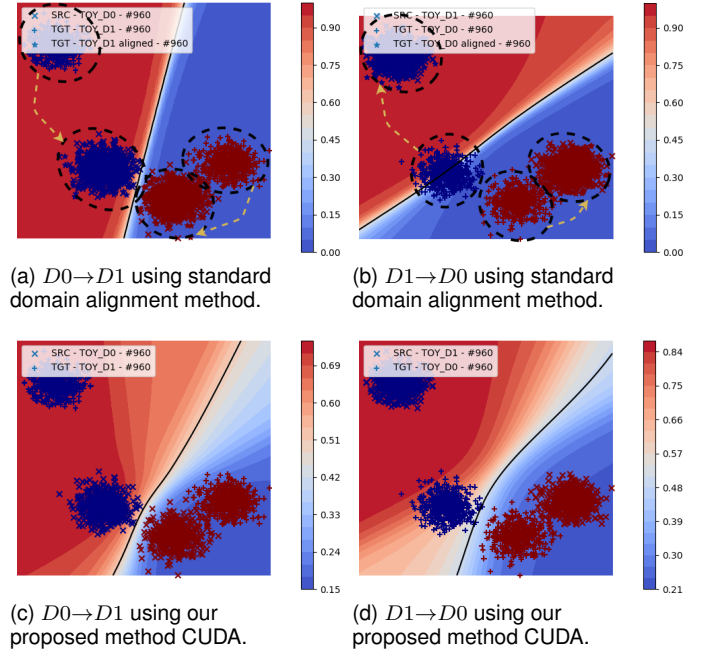


Fig. 1. Demonstration of difference in domain alignment and proposed method CUDA on the 2-dimensional blobs synthetic toy-dataset for domain distributions from popular *scikit-learn* [42]. Top row corresponds to domain alignment approach with two different domains on both $D0 \leftrightarrow D1$ domain adaptation tasks. The yellow dotted lines indicate domain alignment to morph both the domains. Bottom row corresponds to proposed method CUDA in comparison with their respective domain alignment in top row. The two columns indicates the experiments with swapped source and target domains. Unlike domain alignment approach, where the classifier is learnt only on source domain, CUDA demonstrates the contradistinguisher jointly learnt to classify on both the domains. As seen above, swapping domains affects the classifier learnt in domain alignment because the classifier depends on the source domain. However, because of joint learning on both the domains simultaneously, *contradistinguisher* shows almost the same decision boundary irrespective of the source domain. (Best viewed in color.)

by directly learning a single classifier on both source and target domain without domain alignment.

- 6) We analyse learned features using the contradistinguisher loss and their nature. In this recent work [43], it has been established that the ImageNet pre-trained models are biased towards texture and not the shape. A stylized version of ImageNet called *Stylized-ImageNet* [43] is introduced to increase the shape bias of the pre-trained models. However, in our analysis, we observe that model trained using CUDA increases the shape bias over the texture bias of the ImageNet pre-trained feature extractor. This shows that the proposed CUDA inherently tends to learn the most contrastive features in a given sample, which naturally corresponds to the different shapes of the objects without the need of any modified/stylized dataset or ground truth labels as reported in [43].

In Fig 1, we demonstrate the difference between domain alignment and the proposed method CUDA by swapping the domains. One can see that while domain alignment approaches learn classifier only on source domain, the Contradistinguisher jointly learns to classify both the domains. Due to this joint learning we observe an added nice behavior

of obtaining similar classifiers irrespective of the domain being used as the source domain.

The rest of this paper is structured as follows. Section 2 discusses related works in domain adaptation. In Section 3, we elaborate on the problem formulation, neural network architecture used by us, loss functions, model training and inference algorithms, and complexity analysis of our proposed method. Section 4 deals with the discussion of the experimental setup, results and analysis on visual datasets. Finally in Section 5, we conclude by highlighting the key contributions of CUDA.

2 RELATED WORK

As mentioned earlier, almost all domain adaptation approaches rely on domain alignment techniques. Here we briefly outline three main techniques of domain alignment.

(a) *Discrepancy-based methods*: Deep Adaptation Network (DAN) [1] proposes mean-embedding matching of multi-layer representations across domain by minimizing Maximum Mean Discrepancy (MMD) [44], [45], [46] in a reproducing kernel Hilbert space (RKHS). Residual Transfer Network (RTN) [2] introduces separate source and target domain classifiers differing by a small residual function along with fusing the features of multiple layers in a reproducing kernel Hilbert space (RKHS) to match the domain distributions. Joint Adaptation Network (JAN) [3] proposes to optimize Joint Maximum Mean Discrepancy (JMMD), which measures the Hilbert-Schmidt norm between kernel mean embedding of empirical joint distributions of source and target domain. Associative Domain Adaptation (ADA) [4] learns statistically domain invariant embeddings by associating the embeddings of the final fully-connected layer before applying softmax as an alternative to MMD loss. Maximum Classifier Discrepancy (MCD) [5] aligns source and target distributions by maximizing the discrepancy between two separate classifiers. Self Ensembling (SE) [6] uses mean teacher variant [47] of temporal ensembling [48] with heavy reliance on data augmentation to minimize the discrepancy between student and teacher network predictions. Variational Fair Autoencoder (VFAE) [7] uses Variational Autoencoder (VAE) [49] with MMD to obtain domain invariant features. Central Moment Discrepancy (CMD) [8] proposes to match higher order moments of source and target domain distributions. Rozantsev et. al. [9] propose to explicitly model the domain shift using two-stream architecture, one for each domain along with MMD to align the source and target representations. A more recent approach multi-domain Domain Adaptation layer (mDA-layer) [10], [11] proposes a novel idea of replacing standard Batch-Norm layers [50] with specialized Domain Alignment layers [12], [13] thereby reducing the domain shift by discovering and handling multiple latent domains. Geodesic Flow Subspaces (GFS/SGF) [51] performs domain adaptation by first generating two subspaces of the source and the target domains by performing PCA, followed by learning finite number of the interpolated subspaces between source and target subspaces based on the geometric properties of the Grassmann manifold. In the presence of multi-source domains, this method is very effective as this identifies the optimal subspace for domain adaptation.

sFRAME (sparse Filters, Random fields, And Maximum Entropy) [52] models are defined as Markov random field model that model data distributions based as maximum entropy distribution to fit the observed data by identifying the patterns in the observed data. Transferrable Prototypical Networks (TPN) [14] propose to identify prototypes for each class in source and target domains that are close in the embedding space and minimize the distance between these prototypes for domain adaptation.

(b) *Reconstruction-based methods*: Deep Reconstruction-Classification Networks (DRCN) [15] and Domain Separation Networks (DSN) [16] approaches learn a shared encodings of source and target domains using reconstruction networks.

(c) *Adversarial adaptation methods*: Reverse Gradient (RevGrad) [17] or Domain Adversarial Neural Network (DANN) [53] uses domain discriminator to learn domain invariant representations of both the domains. Coupled Generative Adversarial Network (CoGAN) [18] uses Generative Adversarial Network (GAN) [54] to obtain domain invariant features used for classification. Adversarial Discriminative Domain Adaptation (ADDA) [19] uses GANs along with weight sharing to learn domain invariant features. Generate to Adapt (GTA) [20] learns to generate equivalent image in the other domain for a given image, thereby learning common domain invariant embeddings. Cross-Domain Representation Disentangler (CDRD) [21] learns cross-domain disentangled features for domain adaptation. Symmetric Bi-Directional Adaptive GAN (SBADAGAN) [22] aims to learn symmetric bidirectional mappings among the domains by trying to mimic a target image given a source image. Cycle-Consistent Adversarial Domain Adaptation (CyCADA) [23] adapts representations at both the pixel-level and feature-level over the domains. Moving Semantic Transfer Network (MSTN) [24] proposes moving semantic transfer network that learn semantic representations for the unlabeled target samples by aligning labeled source centroids and pseudo-labeled target centroids. Conditional Domain Adversarial Network (CDAN) [25] conditions the adversarial adaptation models on discriminative information conveyed in the classifier predictions. Joint Discriminative Domain Adaptation (JDDA) [26] proposes joint domain alignment along with discriminative feature learning. Decision-boundary Iterative Refinement Training with a Teacher (DIRT-T) [27] and Augmented Cyclic Adversarial Learning (ACAL) [28] learn by using a domain discriminator along with data augmentation for domain adaptation. Deep Cocktail Network (DCTN) [30] proposes a k-way domain discriminator and category classifier for digit classification and real-world object recognition in a multi-source domain adaptation setting. Batch Spectral Penalization (BSP) [31] investigates the transferability and the discriminability of the features learnt using the standard adversarial domain adaptation techniques. Also, BSP proposes an additional batch spectral loss as it is observed that the transferable features learnt using adversarial domain adaptation result in the loss of the discriminability of the classifier. Transferable Normalization (TransNorm) [32] proposes further improvement in transferability by replacing the normal batch-normalization layer with separate normalization layers for source and target domain input batches. Adversarial

Tight Match (ATM) [33] proposes to combine the adversarial training with discrepancy metric by introducing a novel discrepancy metric Maximum Density Divergence (MDD) to minimize inter-domain divergence and maximize the intra-class density. Certainty based Attention for Domain Adaptation (CADA) [34] propose to identify features that increase the certainty of the domain discriminator prediction to improve the classifier. Progressive Feature Alignment Network (PFAN) [35] proposes to align the discriminative features across domains progressively and effectively, via exploiting the intra-class variation in the target domain.

Apart from these approaches, a slightly different method that has been recently proposed is called *Tri-Training*. Tri-Training algorithms use three classifiers trained on the labeled source domain and refine them for unlabeled target domain. To be precise, in each round of tri-training, a target sample is pseudo-labeled if the other two classifiers agree on the labeling, under certain conditions such as confidence thresholding. Asymmetric Tri-Training (ATT) [55] uses three classifiers to bootstrap high confidence target domain samples by confidence thresholding. This way of bootstrapping works only if the source classifier has very high accuracy. In case of low source classifier accuracy, target samples are never obtained to bootstrap, resulting in a bad model. Multi-Task Tri-training (MT-Tri) [56] explores the tri-training technique on the language domain adaptation tasks in a multi-task setting.

All the domain adaptation approaches mentioned earlier have a common unifying theme: they attempt to morph the target and source distributions so as to make them indistinguishable. However, aligning domains is a complex task than the classification task. In this paper, we propose a completely different approach: instead of focusing on aligning the source and target distributions, we learn a single classifier referred as *Contradistinguisher*, jointly on both the domain distributions using contradistinguish loss for the unlabeled target domain data and supervised loss for the labeled source domain data.

3 PROPOSED METHOD: CUDA

A domain \mathcal{D}_d is specified by its input feature space \mathcal{X}_d , the label space \mathcal{Y}_d and the joint probability distribution $p(\mathbf{x}_d, \mathbf{y}_d)$, where $\mathbf{x}_d \in \mathcal{X}_d$ and $\mathbf{y}_d \in \mathcal{Y}_d$. Let $|\mathcal{Y}_d| = K$ be the number of class labels such that $\mathbf{y}_d \in \{0, \dots, K-1\}$ for any instance \mathbf{x}_d . Domain adaptation, in particular, consists of two domains \mathcal{D}_s and \mathcal{D}_t that are referred as the source and target domains respectively. A common assumption in domain adaptation is that the input feature space as well as the label space remains unchanged across the source and the target domain, i.e., $\mathcal{X}_s = \mathcal{X}_t = \mathcal{X}_d$ and $\mathcal{Y}_s = \mathcal{Y}_t = \mathcal{Y}_d$. Hence, the only difference between the source and target domain is input-label space distributions, i.e., $p(\mathbf{x}_s, \mathbf{y}_s) \neq p(\mathbf{x}_t, \mathbf{y}_t)$. This is referred to as *domain shift* in the domain adaptation literature.

In particular, in an unsupervised domain adaptation, the training data consists of labeled source domain instances $\{(\mathbf{x}_s^i, \mathbf{y}_s^i)\}_{i=1}^{n_s}$ and unlabeled target domain instances $\{\mathbf{x}_t^j\}_{j=1}^{n_t}$. Given a labeled data in the source domain, it is straightforward to learn a classifier by maximizing the conditional probability $p(\mathbf{y}_s|\mathbf{x}_s)$ over the labeled samples.

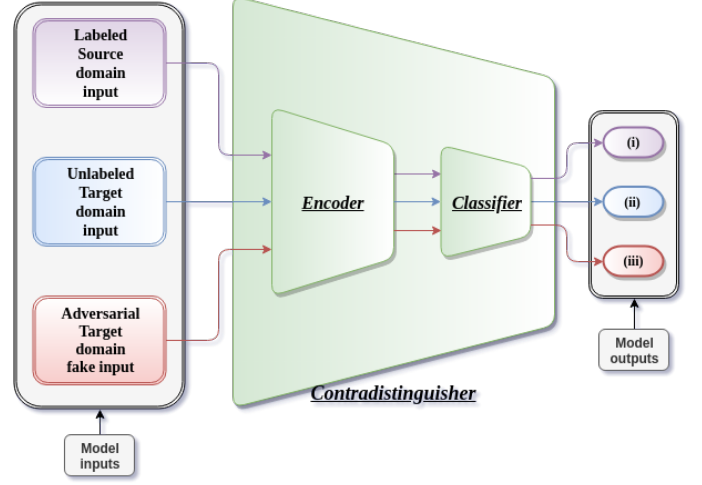


Fig. 2. Architecture of the proposed method CUDA with *Contradistinguisher* (*Encoder* and *Classifier*). Three optimization objectives with their respective inputs involved in training of CUDA: (i) Source supervised (2), (ii) Target unsupervised (5), and Adversarial regularization (9).

However, the task at hand is to learn a classifier on the unlabeled target domain by transferring the knowledge from the labeled source domain.

3.1 Overview

The outline of the proposed method CUDA which involves *contradistinguisher* and the respective losses involved in training are depicted in Fig 2. The objective of *contradistinguisher* is to find a clustering scheme using the most contrastive features on unlabeled target in such a way that it also satisfies the target domain prior, i.e., *prior enforcing*. We achieve this by jointly training on labeled source samples in a supervised manner and unlabeled target samples in an unsupervised end-to-end manner by using a *contradistinguish* loss same as [41].

This fine-tunes the classifier learnt from source domain also to the target domain as demonstrated in Figs 1 and 3. The crux of our approach is the *contradistinguish* loss (5) which is discussed in detail in Section 3.3. Hence, the apt name *contradistinguisher* for our neural network architecture.

Note that the objective of *contradistinguisher* is not same as a classifier, i.e., distinguishing is not same as classifying. Suppose there are two contrastive entities $e_1 \in C_1$ and $e_2 \in C_2$, where C_1, C_2 are two classes. The aim of a classifier is to classify $e_1 \in C_1$ and $e_2 \in C_2$, where to train a classifier one requires labeled data. On the contrary, the job of *contradistinguisher* is to just identify $e_1 \neq e_2$, i.e., *contradistinguisher* can classify $e_1 \in C_1$ (or C_2) and $e_2 \in C_2$ (or C_1) indifferently. To train *contradistinguisher*, we do not need any class information but only need unlabeled entities e_1 and e_2 . Using unlabeled target data, *contradistinguisher* is able to find a clustering scheme by distinguishing the unlabeled target domain samples in an unsupervised way. However, since the final task is classification, one would require a selective incorporation of the pre-existing informative knowledge required for the task of classification. This knowledge of assigning the label to the clusters is obtained by jointly training, thus classifying $e_1 \in C_1$ and $e_2 \in C_2$.

3.2 Supervised Source Classification

For the labeled source domain instances $\{(\mathbf{x}_s^i, \mathbf{y}_s^i)\}_{i=1}^{n_s}$, we define the conditional-likelihood of observing \mathbf{y}_s given \mathbf{x}_s as, $p_\theta(\mathbf{y}_s|\mathbf{x}_s)$, where θ denotes the parameters of contradistinguisher.

We estimate θ by maximizing the conditional log-likelihood of observing the labels given the labeled source domain samples. Therefore, the source domain supervised objective to maximize is given as

$$\mathcal{L}_s(\theta) = \sum_{i=1}^{n_s} \log(p_\theta(\mathbf{y}_s^i|\mathbf{x}_s^i)) . \quad (1)$$

Alternatively, one can minimize the cross-entropy loss, as used in practical implementation, instead of maximizing (1), i.e.,

$$\mathcal{L}_{ce}(\theta) = - \sum_{i=1}^{n_s} \sum_{k=0}^{K-1} \mathbb{1}[\mathbf{y}_s^i=k] \log(\hat{\mathbf{y}}_s^{ik}) , \quad (2)$$

where $\hat{\mathbf{y}}_s^{ik}$ is the softmax output of contradistinguisher that represents the probability of class k for the given sample \mathbf{x}_s^i .

3.3 Unsupervised Target Classification

For the unlabeled target domain instances $\{\mathbf{x}_t^j\}_{j=1}^{n_t}$, as the corresponding labels are unknown, a naive way of predicting the target labels is to directly use the classifier trained only with supervised loss given in (2). While this approach may perform reasonably well in certain cases, it fails to deliver state-of-the-art performance. This may be attributed to the following reason: the support for the distribution p_θ is defined only over the source domain instances \mathbf{x}_s and not the target domain instances \mathbf{x}_t . Hence, we model a non-trivial joint distribution $\hat{q}_\theta(\mathbf{x}_t, \mathbf{y}_t)$ parameterized by the same θ over target domain with only the target domain instances as the support as,

$$\hat{q}_\theta(\mathbf{x}_t, \mathbf{y}_t) = \frac{p_\theta(\mathbf{y}_t|\mathbf{x}_t)}{\sum_{\ell=1}^{n_t} p_\theta(\mathbf{y}_t|\mathbf{x}_t^\ell)} . \quad (3)$$

However (3) is not a joint distribution yet because $\sum_{\ell=1}^{n_t} \hat{q}_\theta(\mathbf{x}_t^\ell, \mathbf{y}_t) \neq p(\mathbf{y}_t)$, i.e., marginalizing over all $\{\mathbf{x}_t^j\}_{j=1}^{n_t}$ does not yield the target prior distribution $p(\mathbf{y}_t)$. We modify (3) so as to include the marginalization condition. Hence, we refer to this as *target domain prior enforcing*.

$$q_\theta(\mathbf{x}_t, \mathbf{y}_t) = \frac{p_\theta(\mathbf{y}_t|\mathbf{x}_t)p(\mathbf{y}_t)}{\sum_{\ell=1}^{n_t} p_\theta(\mathbf{y}_t|\mathbf{x}_t^\ell)} . \quad (4)$$

Note that $q_\theta(\mathbf{x}_t, \mathbf{y}_t)$ defines a non-trivial approximate of joint distribution over the target domain as a function of p_θ learnt over source domain. The resultant unsupervised maximization objective for the target domain is given by maximizing the log-probability of the joint distribution $q_\theta(\mathbf{x}_t, \mathbf{y}_t)$ which is

$$\mathcal{L}_t(\theta, \{\mathbf{y}_t^j\}_{j=1}^{n_t}) = \sum_{j=1}^{n_t} \log(q_\theta(\mathbf{x}_t^j, \mathbf{y}_t^j)) . \quad (5)$$

Next, we discuss how the objective given in (5) is solved and the reason why (5) is referred as contradistinguish loss. Since the target labels $\{\mathbf{y}_t^j\}_{j=1}^{n_t}$ are unknown, one needs to maximize (5) over the parameters θ as well as the unknown

target labels \mathbf{y}_t . As there are two unknown variables for maximization, we follow a two step approach to maximize (5) as analogous to Expectation Maximization (EM) algorithm [57]. The two optimization steps are as follows.

(i) *Pseudo-label selection*: We maximize (5) only with respect to the label \mathbf{y}_t for every \mathbf{x}_t by fixing θ as

$$\hat{\mathbf{y}}_t^j = \arg \max_{\mathbf{y}^j \in \mathcal{Y}_t} \frac{p_\theta(\mathbf{y}^j|\mathbf{x}_t^j)p(\mathbf{y}_t)}{\sum_{\ell=1}^{n_t} p_\theta(\mathbf{y}^\ell|\mathbf{x}_t^\ell)} . \quad (6)$$

Pseudo-labeling approach under semi-supervised representation learning setting has been well studied in [58] and shown equivalent to *entropy regularization* [59]. As previously mentioned, pseudo-label selection is analogous to E-step in EM algorithm. Moreover, we derive the motivation from [41] that also uses pseudo-labeling in the context of semi-supervised representation learning. However, the proposed method addresses a more complex problem of domain adaptation in the presence of domain shift. The pseudo-labeling essentially tries to cluster by assigning labels using source domain features of the classifier trained on the source domain. This effectively is similar to the E-step in EM algorithm in spirit.

(ii) *Maximization*: By fixing the pseudo-labels $\{\hat{\mathbf{y}}_t^j\}_{j=1}^{n_t}$ from (6), we train contradistinguisher to maximize (5) with respect to the parameter θ .

$$\begin{aligned} \mathcal{L}_t(\theta) &= \sum_{j=1}^{n_t} \log(p_\theta(\hat{\mathbf{y}}_t^j|\mathbf{x}_t^j)) + \sum_{j=1}^{n_t} \log(p(\mathbf{y}_t)) \\ &\quad - \sum_{j=1}^{n_t} \log\left(\sum_{\ell=1}^{n_t} p_\theta(\hat{\mathbf{y}}_t^j|\mathbf{x}_t^\ell)\right) . \end{aligned} \quad (7)$$

Since the pseudo-labels from (6) are used for the maximization, this constraints the model to learn the features to further improve the current pseudo-labeling for the next iteration. This step is similar to the M-step in EM algorithm in spirit.

The first term, i.e., log-probability for a label $\hat{\mathbf{y}}_t^j$ given \mathbf{x}_t^j forces contradistinguisher to choose features to classify \mathbf{x}_t^j to $\hat{\mathbf{y}}_t^j$. The second term is a constant, hence it has no effect on the optimization with respect to θ . The third term is the negative of log-probability for the label $\hat{\mathbf{y}}_t^j$ given all the samples \mathbf{x}_t in the entire domain. Maximization of this term forces contradistinguisher to choose features to not classify all the other $\mathbf{x}_t^{\ell \neq j}$ to selected pseudo-label $\hat{\mathbf{y}}_t^j$ except the given sample \mathbf{x}_t^j . This forces contradistinguisher to extract the most unique features of a given sample \mathbf{x}_t^j against all the other samples $\mathbf{x}_t^{\ell \neq j}$, i.e., most unique contrastive feature of the selected sample \mathbf{x}_t^j over all the other samples $\mathbf{x}_t^{\ell \neq j}$ to distinguish a given sample from all others.

The first and third term together in (7) enforce that contradistinguisher learns the most contradistinguishing features among the samples $\mathbf{x}_t \in \mathcal{X}_t$, thus performing unlabeled target domain classification in a fully unsupervised way. Because of this contradistinguishing feature learning, we refer the unsupervised target domain objective (5) as contradistinguish loss.

Ideally, one would like to compute the third term in (7) using the complete target training data for each input sample. Since it is expensive to compute the third term over the entire \mathbf{x}_t for each individual sample during training,

one evaluates the third term in (7) over a mini-batch. In our experiments, we have observed that mini-batch strategy does not cause any problem during training as far as it includes at least one sample from each class which is fair assumption for a reasonably large mini-batch size of 128. For numerical stability, we use $\log \sum \exp$ trick to optimize third term in (7).

3.4 Adversarial Regularization

In order to prevent contradistinguisher from over-fitting to the chosen pseudo labels during the training, we use adversarial regularization. In particular, we train contradistinguisher to be confused about set of fake negative samples $\{\hat{\mathbf{x}}_t^j\}_{j=1}^{n_f}$ by maximizing the conditional log-probability over the given fake sample such that the sample belongs to all $K(|\mathcal{Y}_d|)$ classes simultaneously. The objective of the adversarial regularization is to multi-label the fake sample (e.g., noisy image that looks like a cat and a dog) equally to all K classes as labeling to any unique class introduces more noise in pseudo labels. This strategy is similar to entropy regularization [59] in the sense that instead of minimizing the entropy for the real target samples, we maximize the conditional log-probability over the fake negative samples. Therefore, we add the following maximization objective to the total contradistinguisher objective as a regularizer.

$$\mathcal{L}_{adv}(\theta) = \sum_{j=1}^{n_f} \log(p_\theta(\hat{\mathbf{y}}_t^j | \hat{\mathbf{x}}_t^j)) , \quad (8)$$

for all $\hat{\mathbf{y}}_t^j \in \mathcal{Y}_t$. As maximization of (8) is analogous to minimizing the binary cross-entropy loss (9) of a multi-class multi-label classification task, in our practical implementation, we minimize (9) for assigning labels to all the classes for every sample.

$$\mathcal{L}_{bce}(\theta) = - \sum_{j=1}^{n_f} \sum_{k=0}^{K-1} \log(\hat{\mathbf{y}}_t^{jk}) , \quad (9)$$

where $\hat{\mathbf{y}}_t^{jk}$ is the softmax output of contradistinguisher which represents the probability of class k for the given sample $\hat{\mathbf{x}}_t^j$.

The fake negative samples $\hat{\mathbf{x}}_t$ can be directly sampled from, say a Gaussian distribution in the input feature space \mathcal{X}_t with the mean and standard deviation of the samples $\mathbf{x}_t \in \mathcal{X}_t$. For the language domain, fake samples are generated randomly as mentioned above because the input feature is the form of embeddings extracted from denoising auto-encoder with bag-of-words as the auto-encoder's input. In case of visual datasets, as the feature space is high dimensional, the fake images $\hat{\mathbf{x}}_t$ are generated using a generator network G_ϕ with parameter ϕ that takes Gaussian noise vector η_t as input to produce a fake sample $\hat{\mathbf{x}}_t$, i.e., $\hat{\mathbf{x}}_t = G_\phi(\eta_t)$. Generator G_ϕ is trained by minimizing kernel-MMD loss [60], i.e., a modified version of MMD loss be-

tween the encoder output $\rho_{enc}(\hat{\mathbf{x}}_t)$ and $\rho_{enc}(\mathbf{x}_t)$ of n_f fake images $\hat{\mathbf{x}}_t$ and n_t real target domain images \mathbf{x}_t respectively.

$$\begin{aligned} \mathcal{L}_{gen}(\phi) = & \frac{1}{n_f^2} \sum_{i=1}^{n_f} \sum_{j=1}^{n_f} k(\rho_{enc}(\hat{\mathbf{x}}_t^i), \rho_{enc}(\hat{\mathbf{x}}_t^j)) \\ & + \frac{1}{n_t^2} \sum_{i=1}^{n_t} \sum_{j=1}^{n_t} k(\rho_{enc}(\mathbf{x}_t^i), \rho_{enc}(\mathbf{x}_t^j)) \\ & - \frac{2}{n_t n_f} \sum_{i=1}^{n_f} \sum_{j=1}^{n_t} k(\rho_{enc}(\hat{\mathbf{x}}_t^i), \rho_{enc}(\mathbf{x}_t^j)), \quad (10) \end{aligned}$$

where $k(x, x') = e^{-\gamma \|x - x'\|^2}$ is the Gaussian kernel.

Note that the objective of the generator is not to generate realistic images but to generate fake noisy images with mixed image attributes from the target domain. This reduces the effort of training powerful generators which is the focus in adversarial based domain adaptation approaches [20], [21], [22], [23], [24] used for domain alignment.

3.5 Algorithms and Complexity Analysis

Algorithm 1 and 2 list steps involved in CUDA training and inference respectively. Further, we briefly discuss the time complexity of Algorithm 1 and 2. We also compare model complexity of CUDA against domain alignment approaches.

(a) *Time complexity*: We consider a batch of b instances for forward and backward propagation during training. For computing source supervised loss given in (2), the time complexity is $O(bKT_c)$, where T_c is the time complexity involved in obtaining the classifier output which mainly depends on the model complexity which will be discussed next. For computing target unsupervised loss given in (5), the time complexity is $O(bKT_c)$ for pseudo-label selection and $O(b^2KT_c)$ for first and third terms in maximization step, i.e., $O(b^2KT_c)$ effectively for the target unsupervised loss (5). The adversarial regularization loss in (9) has the time complexity $O(bKT_c)$. Time complexity for generator training is $O(b^2D_eT_e)$, where D_e is dimension of the encoder output and T_e is the time complexity of the encoder neural network which also depends on the model complexity discussed next. As T_c dominates T_e , total training time complexity can be further simplified to $O(b^2KT_c)$ per mini-batch with a patience based early-stopping on loss over the held-out validation set. During inference phase, the time complexity is $O(n_{test}T_c)$, where n_{test} is the number of inference samples.

(b) *Model complexity*: As discussed above, T_c mainly depends on the model complexity involving many factors such as input feature dimension, number of neural network layers, type of normalization, type of activation functions etc. Contradistinguisher is a simple network with a single encoder and classifier unlike MCD [5] that uses a single encoder with two classifier. This makes MCD [5] time complexity $2T_c$ instead of just T_c . Similarly, SE [6] uses 2 copies of network of encoder and classifier one for student and other for teacher network. This makes SE [6] time complexity $2T_c$ instead of T_c . In general, as domain alignment approaches use additional circuitry either in terms of multiple classifiers or GANs, the model complexity

Algorithm 1: CUDA Training

Input: $b=batch_size, epochs=max_epoch,$
 $n_{batch}=number\ of\ batches$
Output: θ // parameter of contradistinguisher
Data: $\{(\mathbf{x}_s^i, \mathbf{y}_s^i)\}_{i=1}^{n_s}, \{\mathbf{x}_t^j\}_{j=1}^{n_t}$

- 1 **if** target domain prior $p(\mathbf{y}_t)$ is known **then**
- 2 use $p(\mathbf{y}_t)$ for the contradistinguish loss (5)
 // target domain prior enforcing
- 3 **else**
- 4 compute $p(\mathbf{y}_t)$ assuming $p(\mathbf{y}_t) = p(\mathbf{y}_s)$ // fair
 assumption as most datasets are well
 balanced
- 5 **for** $epoch = 1$ to $epochs$ **do**
- 6 **for** $batch = 1$ to n_{batch} **do**
- 7 sample a mini-batch $\{(\mathbf{x}_s^i, \mathbf{y}_s^i)\}_{i=1}^b, \{\mathbf{x}_t^j\}_{j=1}^b$
- 8 compute $\mathcal{L}_s(\theta)$ (1) using $\{(\mathbf{x}_s^i, \mathbf{y}_s^i)\}_{i=1}^b$
 // source supervised loss
- 9 compute $\{\hat{\mathbf{y}}_t^j\}_{j=1}^b$ (6) using $\{\mathbf{x}_t^j\}_{j=1}^b$ // pseudo
 label selection step
- 10 compute $\mathcal{L}_t(\theta)$ (7) fixing $\{\hat{\mathbf{y}}_t^j\}_{j=1}^b$
 // maximization step
- /* steps 9 and 10 together optimize
 unsupervised contradistinguish loss (5)
 */
- 11 **if** adversarial regularization is enabled **then**
- 12 **if** Generator G_ϕ is used **then**
- 13 get fake samples $\{\hat{\mathbf{x}}_t^j\}_{j=1}^b$ from
 Gaussian noise vectors $\{\eta_t^j\}_{j=1}^b$ using
 G_ϕ , compute $\mathcal{L}_{gen}(\phi)$ (10)
 // generator training
- 14 **else**
- 15 get fake samples $\{\hat{\mathbf{x}}_t^j\}_{j=1}^b$ by random
 sampling in the input feature space \mathcal{X}_t
- 16 compute $\mathcal{L}_{adv}(\theta)$ (9) using $\{\hat{\mathbf{x}}_t^j\}_{j=1}^b$
 // fake samples are assigned to all
 classes equally
- 17 combine losses in steps 8,10,13, and 16 to
 compute gradients using back-propagation
- 18 update θ using gradient descent // and ϕ if
 G_ϕ is used

Algorithm 2: CUDA Inference

Input: $\{\mathbf{x}_{test}^i\}_{i=1}^{n_{test}}$ // input test samples
Output: $\{\hat{\mathbf{y}}_{test}^i\}_{i=1}^{n_{test}}$ // predicted labels

- 1 **for** $i = 1$ to n_{test} **do**
- 2 predict label as $\hat{\mathbf{y}}_{test}^i = \arg \max_{\mathbf{y} \in \mathcal{Y}_t} p_\theta(\mathbf{y} | \mathbf{x}_{test}^i)$

increases at least by a factor of 2. This increased model complexity requires more data augmentation to prevent overfitting leading to further increases in time complexity at the expense of only a slight improvement, if any, compared to CUDA as indicated by our state-of-the-art results without any data augmentation in both visual and language domain

adaptation tasks. We believe the trade-off achieved by the simplicity of CUDA, as evident from our results, is very desirable compared to most domain alignment approaches that use data augmentation and complex neural networks for a slight improvement, if any.

3.6 Extension to Multi-Source Domain Adaptation

Here, we argue that our proposed method CUDA has implicit advantage in dealing with multi-source domain adaption problems over the techniques that are based on domain alignment. In multi-source domain adaption setting, domain alignment methods not only need to consider the domain-shift between source and target domain but also consider the domain-shift between the multiple source domains. Therefore, domain alignment methods are required to solve even more complex intermediate problem of aligning multiple source and target domain distributions in addition to the complex intermediate problem of source and target domain alignment to deal with the multi-source domain adaptation problems. However, as the proposed method does not depend on the domain alignment, the extension to multi source in the proposed method is very simple. As our main focus is to perform unsupervised learning directly on the target domain, the model obtained using is better generalized to the target domain and reduces overfitting on the source source which usually results in a negative transfer. We believe that this is one of the main advantages of addressing the domain adaptation by performing the primary task of target domain classification rather than intermediate task of domain alignment.

We propose a simple extension our proposed method to perform multi-source domain adaptation in the following manner. Let us suppose we are given with R source domains $\{s_1, \dots, s_R\}$, consisting of labeled training data $(\{(\mathbf{x}_{s_1}^i, \mathbf{y}_{s_1}^i)\}_{i=1}^{n_{s_1}}, \dots, \{(\mathbf{x}_{s_R}^i, \mathbf{y}_{s_R}^i)\}_{i=1}^{n_{s_R}})$ and unlabeled target domain instances $\{\mathbf{x}_t^j\}_{j=1}^{n_t}$. We compute the source supervised loss for the r^{th} source domain using (2), i.e., $\mathcal{L}_{s_r}(\theta)$ (1) with $\{(\mathbf{x}_{s_r}^i, \mathbf{y}_{s_r}^i)\}_{i=1}^{n_{s_r}}$ training data. We further compute the total multi-source supervised loss as

$$\mathcal{L}_{s_{total}}(\theta) = \sum_{r=1}^R \mathcal{L}_{s_r}(\theta). \quad (11)$$

We replace $\mathcal{L}_s(\theta)$ (1) in the total optimization objective with $\mathcal{L}_{s_{total}}(\theta)$ (11) in step 17 of Algorithm 1. It should be noted that the unsupervised loss for the target domain is still unmodified irrespective of the number of source domains.

4 EXPERIMENTS

For our domain adaptation experiment, we consider both synthetic and real-world datasets. Under synthetic datasets, we experiment using 2-dimensional blobs with different source and target domain probability distributions to demonstrate the effectiveness of the proposed method under different domain shifts. Under real-world datasets, we consider the complex high resolution Office-31 [39] and VisDA-2017 [40] object classification datasets for our experiment as the low resolution datasets are already addressed in our conference paper CUDA: Contradistinguisher for Unsupervised Domain Adaptation (CUDA) [38].

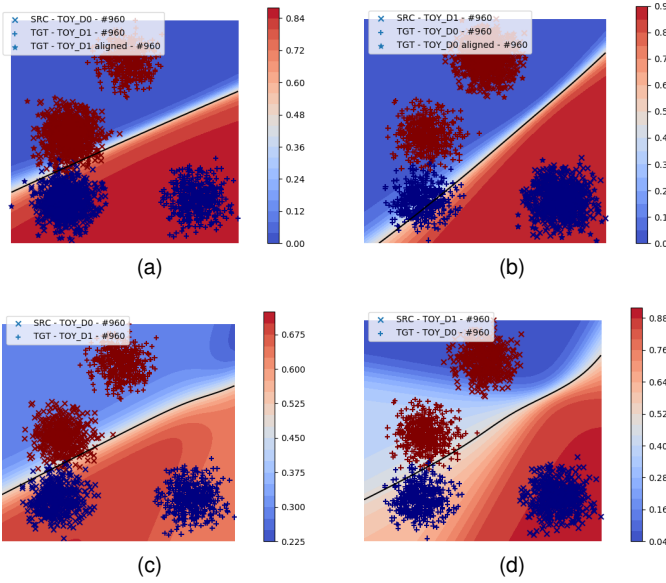


Fig. 3. Additional demonstration of difference in domain alignment and proposed method CUDA on synthetic toy-datasets using blobs similar to Fig 1. Top row corresponds to domain alignment approach with two different domains in both $TOY_D0 \leftrightarrow TOY_D1$ domain adaptation tasks. Bottom row corresponds to the proposed method CUDA in comparison with their respective domain alignment method in top row. As seen above, swapping domains affects the classifier learnt in domain alignment methods because the classifier depends on the source domain. However, because of joint learning on both the domains simultaneously in the proposed method CUDA, *contradistinguisher* shows almost the same decision boundary irrespective of the source domain when the domains are swapped. (Best viewed in color.)

Table 1 provides details on the visual datasets used in our experiments. We have published our python code for all the experiments at <https://github.com/sobalgi/cuda>, originally derived from DisCoder [41] at <https://github.com/gauravpandeyamu/DisCoder>.

4.1 Experiments on Synthetic Toy-dataset

We validate our proposed method by performing experiments on synthetically created simple datasets that model different source and target domain distributions in a 2-dimensional input feature space using different blobs of source-target domain orientations and offsets (i.e., domain shift). We create blobs for source and target domains with 4000 samples using standard *scikit-learn* [42] as indicated in Figs 1 and 3. We further evenly split these 4000 data-points into equal train and test sets. Each of the splits consists the same number of samples corresponding to both the class labels.

The main motivation of the experiments on toy-dataset is to understand and visualize the behavior of the proposed method under some typical domain distribution scenarios and analyse the performance of CUDA. *Blobs* toy-dataset plots in Fig 3 shows clear comparisons of the classifier decision boundaries learnt using CUDA over domain alignment approaches. The top row in Fig 3 corresponds to domain alignment classifier trained only on the labeled source domain, i.e., ss . However, the bottom row in Fig 3 corresponds to *contradistinguisher* trained using the proposed method

TABLE 1
Details of visual datasets.

Dataset	# Train	# Test	# Classes	Target	Resolution
US [61]	7,291	2,007	10	Digits	$1 \times 16 \times 16$
MN [62]	60,000	10,000	10	Digits	$1 \times 28 \times 28$
SV [63]	73,257	26,032	10	Digits	$3 \times 32 \times 32$
SN [17]	479,400	9,553	10	Digits	$3 \times 32 \times 32$
$C9$ [64]	45,000	9,000	9	Object ID	$3 \times 32 \times 32$
$S9$ [65]	4,500	7,200	9	Object ID	$3 \times 96 \times 96$
SS [17]	100,000	-	43	Traffic Signs	$3 \times 40 \times 40$
GT [66]	39,209	12,630	43	Traffic Signs	$3 \times 40 \times 40$
\mathcal{A} [39]	2,817	-	31	Objects	$3 \times 224 \times 224$
\mathcal{D} [39]	498	-	31	Objects	$3 \times 224 \times 224$
\mathcal{W} [39]	795	-	31	Objects	$3 \times 224 \times 224$
\mathcal{V}_{syn} [40]	152,397	-	12	Objects	$3 \times 224 \times 224$
\mathcal{V}_{real} [40]	55,388	72,372	12	Objects	$3 \times 224 \times 224$

CUDA with labeled source and unlabeled target domain, i.e., $ss+tu+ta$.

Fig 4 demonstrates the classifier learnt using CUDA on the synthetic datasets with different complex shapes and orientations of the source and target domain distributions for the input data. Figs 1c and 3c indicates the simplest form of the domain adaptation tasks where are domains have similar orientations in source and target domain distributions. It is important to note that the prior enforcing used in pseudo-label selection is the reason such fine classifier boundaries are observed especially in Figs 1d, 3d, and 4a-4e. Figs 4f and 4g represents more complex configurations of source and target domain distributions that indicate the hyperbolic decision boundaries jointly learnt on both the domains simultaneously using a single classifier without explicit domain alignment. Similarly, Fig 4h represents a complex configuration of source and target domain distributions that indicates an elliptical decision boundary.

4.2 Experiments on Real-world Datasets

Under real-world datasets, we consider the complex high resolution Office-31 [39] and VisDA-2017 [40] object classification datasets for domain adaptation.

4.2.1 Office-31 Dataset

In high resolution visual datasets, we consider Office-31 [39] dataset for our experiments. Unlike low resolution visual datasets, here we have only few hundreds of training samples which makes this an even more challenging task.

Office objects: Office-31 [39] dataset consists of high resolution images of objects belonging to 31 classes obtained from three different domains AMAZON (\mathcal{A}), DSLR (\mathcal{D}), and WEBCAM (\mathcal{W}). Fig 5 shows illustrations of the images from all the three above mentioned domains of the Office-31 [39] dataset. AMAZON (\mathcal{A}) domain consists of synthetic images with clear white background. DSLR (\mathcal{D}) and WEBCAM (\mathcal{W}) domains consist of real-world images with noisy background and surroundings. We consider all possible six combinatorial tasks of domain adaptation involving all the three domains, i.e., $\mathcal{A} \leftrightarrow \mathcal{D}$, $\mathcal{A} \leftrightarrow \mathcal{W}$ and $\mathcal{D} \leftrightarrow \mathcal{W}$. Compared to low resolution visual datasets, Office-31 [39] dataset domain

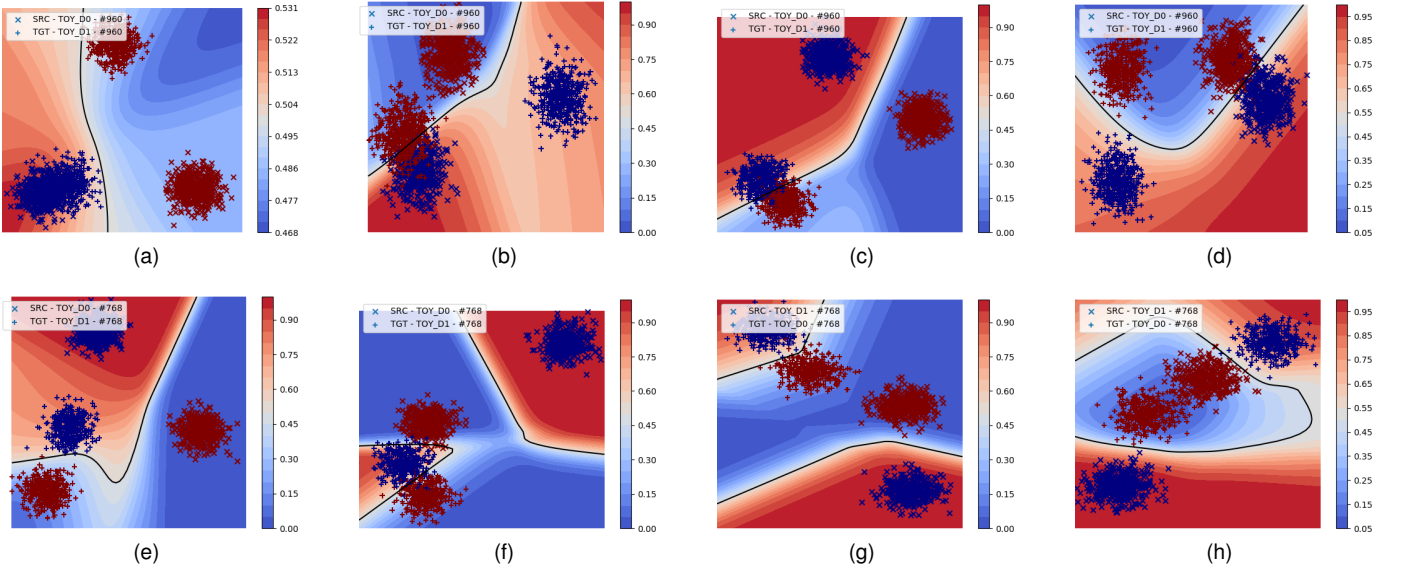


Fig. 4. Contour plots show the probability contours along with clear decision boundaries on different toy-dataset settings trained using CUDA. (source domain: \times , target domain: $+$, class 0: blue, class 1: red.) (Best viewed in color.)

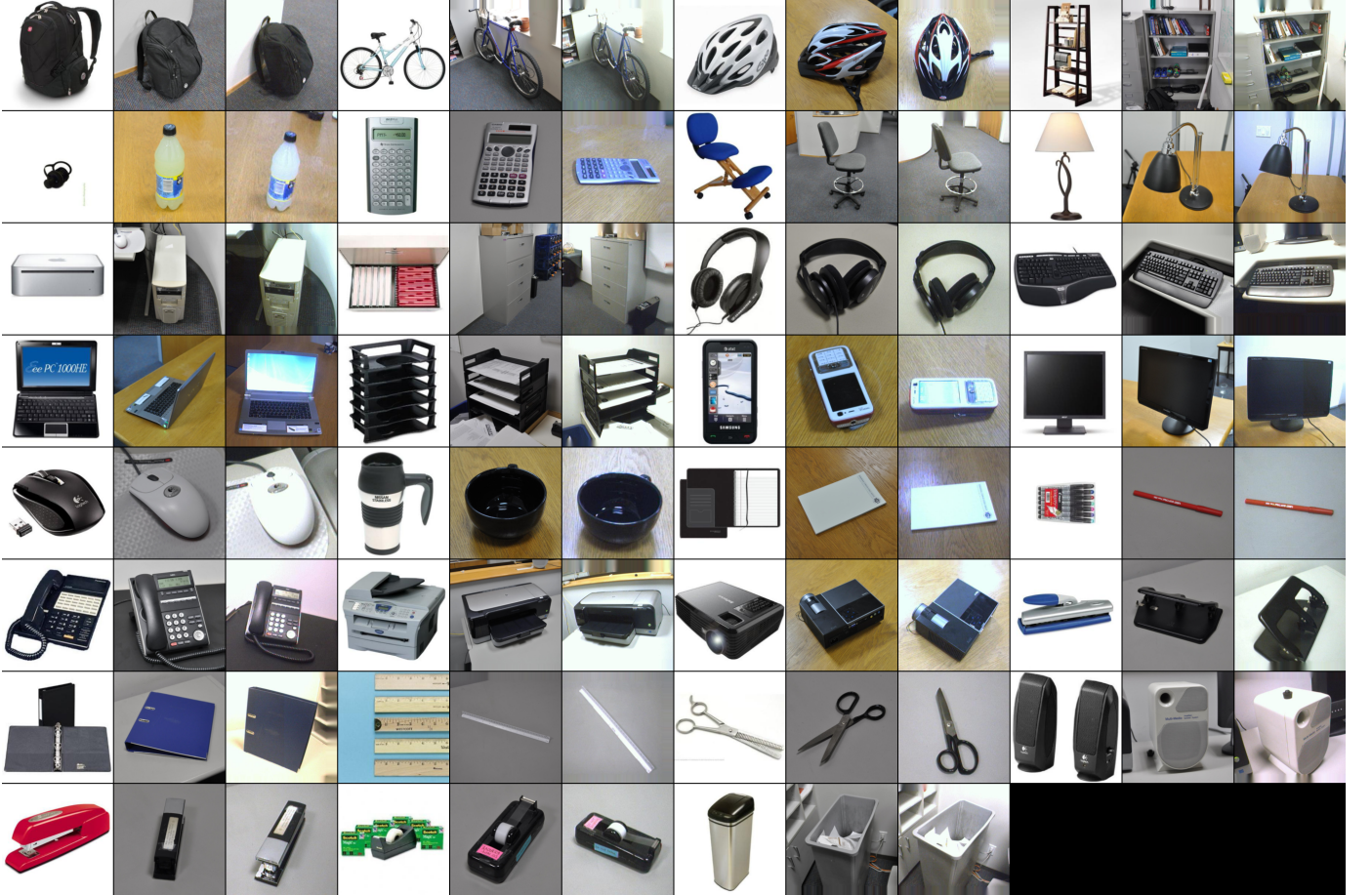


Fig. 5. Illustrations of samples from all the three domains of high resolution Office-31 [39] dataset with one instance per each class from every domain (column $\{1,4,7,10\}$: \mathcal{A} , $\{2,5,8,11\}$: \mathcal{D} , $\{3,6,9,12\}$: \mathcal{W}). (Best viewed in color.)

adaptation tasks have increased complexity due to the small number of training images. To alleviate the lack of large number of training samples, pre-trained networks such as

ResNet-50 [67] and ResNet-152 [67] were used to extract 2048 dimensional features from high resolution images similar to CDAN [25]. Since the images are not well centered

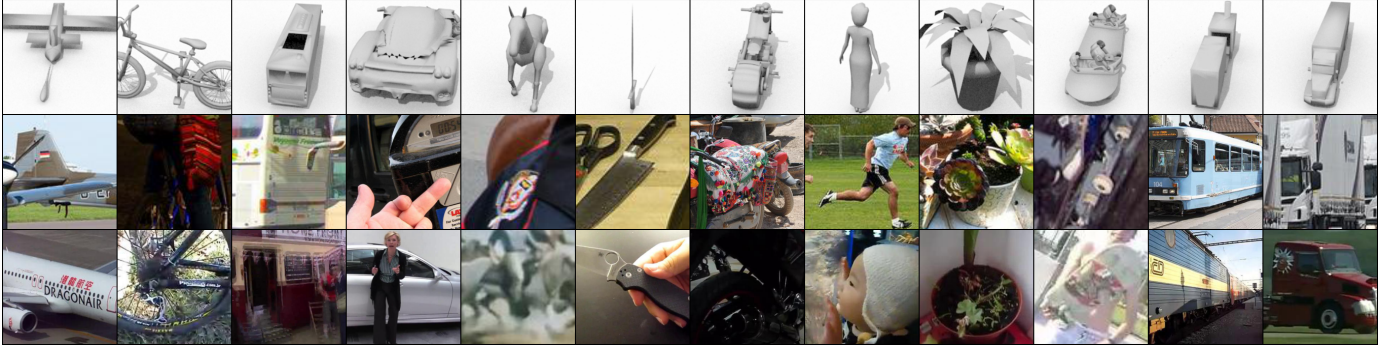


Fig. 6. Illustrations of samples from all the three data-splits of VisDA-2017 [40] dataset with one instance per each class from every domain ($\{\text{row } 1\}$: V_{syn} source domain synthetic images (training set), $\{\text{row } 2\}$: V_{real} target domain real-world images (validation set), $\{\text{row } 3\}$: V_{real} target domain real-world images (testing set)). (Best viewed in color.)

and have a high resolution, we use the standard ten-crop of the image to extract features from the same images during training and testing, also similar to CDAN [25].

The use of pre-trained models leads to two choices of training, (i) Fine-tune the pre-trained model used as feature extractor along with the final classifier layer: This requires careful selection of several hyper-parameters such as learning rate, learning rate decay, batch size etc. to fine-tune the network to the current dataset while preserving the ability of the pre-trained network. We observed that fine-tuning also depends on the loss function used for training [68], which in our case the use of contradistinguish loss greatly affected the changes in the pre-trained model as it is trained only using cross-entropy loss. Fine-tuning also computationally expensive and time-consuming as each iteration requires computing gradients of all the parameters of the pre-trained model. (ii) Fix the pre-trained model and only train the final classifier layer: Alternative to fine-tuning is to fix the pre-trained model and use it only as a feature extractor. This approach has multiple practical benefits such as, (a) The computational time and cost of the fine-tuning the parameters of pre-trained model is alleviated. (b) Since the feature extractor is fixed, it requires only once to extract and store the features locally instead of extracting the same features every iteration. Hence reducing the training time and the GPU memory as it is only required to train the final classifier.

4.2.2 VisDA-2017 Dataset

The VisDA-2017 dataset consists of two domains, (i) synthetic and (ii) real with three predefined data splits. The three predefined data splits in VisDA-2017 dataset are as follows.

(i) Training set: This split includes of 152,397 labeled synthetic images obtained using 2D renderings of 3D models from different angles and different lighting conditions. This split is considered as labeled source domain for training.

(ii) Validation set: This split includes of 55,388 real-world images obtained from curated subset of MS COCO [69] dataset. This split is considered as unlabeled target domain training set and is used during the training without labels.

(iii) Testing set: This split includes of 72,372 real-world images obtained from YouTube Bounding Boxes [70] dataset. This split is considered as target domain testing set

used for evaluation and to report the results. Fig 6 indicates the samples from all the 12 classes of the three data splits.

For experiments on VisDA-2017 dataset, we consider the most recent state-of-the-art benchmark domain adaptation approach BSP [31]. Like BSP, we use the same neural network architecture with pre-trained ResNet-101 with contradistinguish loss for training. BSP reports the evaluation metric of accuracy in the paper. However, during the exercise of results reproduction from BSP¹ to set the baseline for comparison, it was found that the results reported had these following inconsistencies.

- 1) The results reported in the paper as accuracy in actual were the class-wise recall scores.
- 2) Normally the experimental results are reported on the test split which is unseen during the training. However, in BSP, the results are reported on the validation set which is used as the unlabeled target domain training set. Since, the VisDA-2017 dataset has pre-defined splits for evaluation, reporting the results on validation set used during the training might not indicate the generalization of the unseen test set.

4.3 Experimental Results on Real-world Datasets

In our earlier conference paper [38], we have demonstrated the effectiveness of CUDA in domain adaptation on low resolution visual datasets and language datasets. In contrast to low resolution visual datasets, high resolution Office-31 [39] dataset does not have separate pre-defined train and test splits. Since we do not use any labels from the target domain during training, we report ten-crop test accuracy on the target domain by summing the softmax values of all the ten crops of the image and assign the label with maximum aggregate softmax value for the given image as in CDAN [25] in Table 2. In Table 3, we report the target domain accuracy similar to Table 2 in a multi-source domain adaptation setting by combining two domains into a single labeled source domain and the remaining domain as the unlabeled target domain. In Table 3, the indicated multi-source setting baseline results [1], [10], [13], [17], [30], [51], [52] are reported from the published results of [10].

Apart from the standard domain alignment methods used for comparison, we report the performance of two

1. <https://github.com/thuml/Batch-Spectral-Penalization>

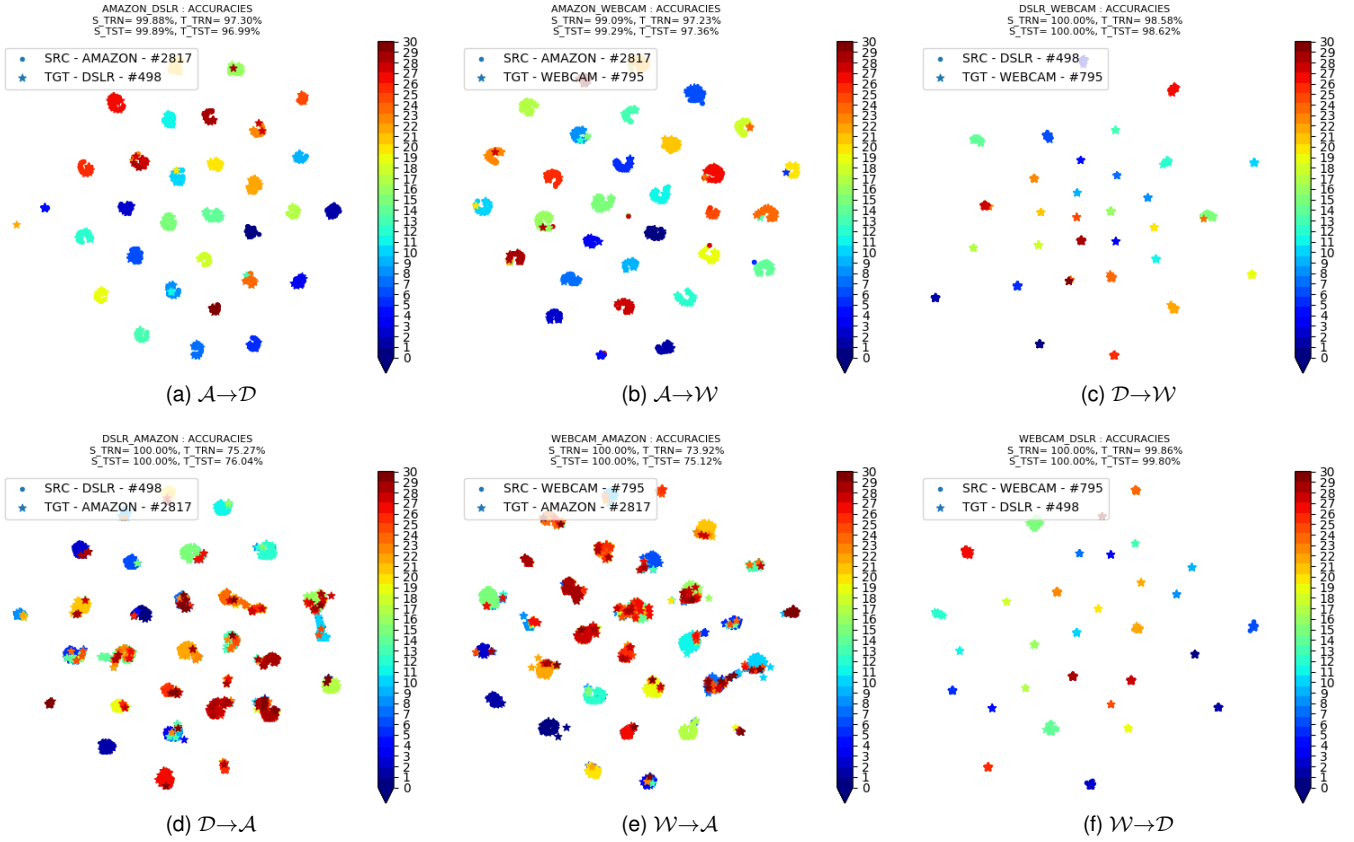


Fig. 7. t-SNE [71] plots for embeddings from the output of contradistinguisher with samples from Office-31 [39] dataset as input corresponding to the highest mean accuracy setting $ss+tu+su+ta$ indicated in Table 2 using ResNet-152 [67] as the fixed encoder. We can observe the clear class-wise clustering of among all the 31 classes in the Office-31 [39] datasets. We achieve high accuracies in spite of having only few hundred training samples in each domain. (Best viewed in color.)

baselines \mathcal{BL}_1 and \mathcal{BL}_2 of our own, in Tables 2, and 3, by fixing the contradistinguisher neural network architecture and varying only the training losses. \mathcal{BL}_1 involves training contradistinguisher using only the source domain in a fully supervised way. \mathcal{BL}_2 involves training contradistinguisher using only the target domain in a fully supervised way. \mathcal{BL}_1 and \mathcal{BL}_2 respectively indicates the minimum and maximum target domain test accuracy that can be attained with chosen contradistinguisher neural network. Comparing CUDA with \mathcal{BL}_1 in Tables 2, and 3, we can see huge improvements in the target domain test accuracies due to the use of contradistinguisher loss (5) demonstrating the effectiveness of contradistinguisher. As our method is mainly dependent on the contradistinguisher loss (5), by experimenting with better neural networks along with our contradistinguisher loss (5), we observed improved results over neural networks of [5], [19] on low resolution visual experiments. We used ResNet over AlexNet on high resolution visual experiments.

4.4 Analysis of Experimental Results

4.4.1 Office-31 Dataset Single-Source Domain Adaptation Results

We report the standard ten-crop accuracy on the target domain images as reported by several state-of-the-art domain adaptation methods [3], [20], [25]. Since there are no explicit test split specified in the dataset and no labels are used from

the target domain during training, it is common to report ten-crop accuracy considering the whole target domain.

In Table 2, we report accuracies obtained by fine-tuning ResNet-50 [67] using the learning rate scheduling followed in CDAN [25] and also without fine-tuning ResNet-50 [67]. Apart from fixed ResNet-50 [67], we also report accuracies with fixed ResNet-152 [67] in Table 2 for comparison. Figs 7a-7f indicate the t-SNE [71] plots of the softmax output after aggregating the ten-crop of each image corresponding to training configuration $ss+tu+su+ta$ reported in Table 2. Fig 7 reports the t-SNE [71] plots of the training setting using ResNet-152 [67] encoder with the highest mean accuracy of all the six domain adaptation tasks. We clearly observe that CUDA outperforms several state-of-the-art methods that also use ResNet-50 [67] and even further surpasses by using ResNet-152 [67] encoder with CUDA. From our ablations study in Table 2, we show the effect of selection of ImageNet pre-trained ResNet-50 and ResNet-152 models on the domain adaptation with similar implications with the work [72].

Among the three domains in Office-31 [39] dataset, \mathcal{A} can be considered as well curated synthetic dataset with clear background and $\{\mathcal{D}, \mathcal{W}\}$ as uncured real-world dataset with noisy background and surroundings. We report the six domain adaptation tasks in the order of their complexity from low to high as, (i) Figs 7c and 7f indicate highest accuracies because of similar real-world to real-world do-

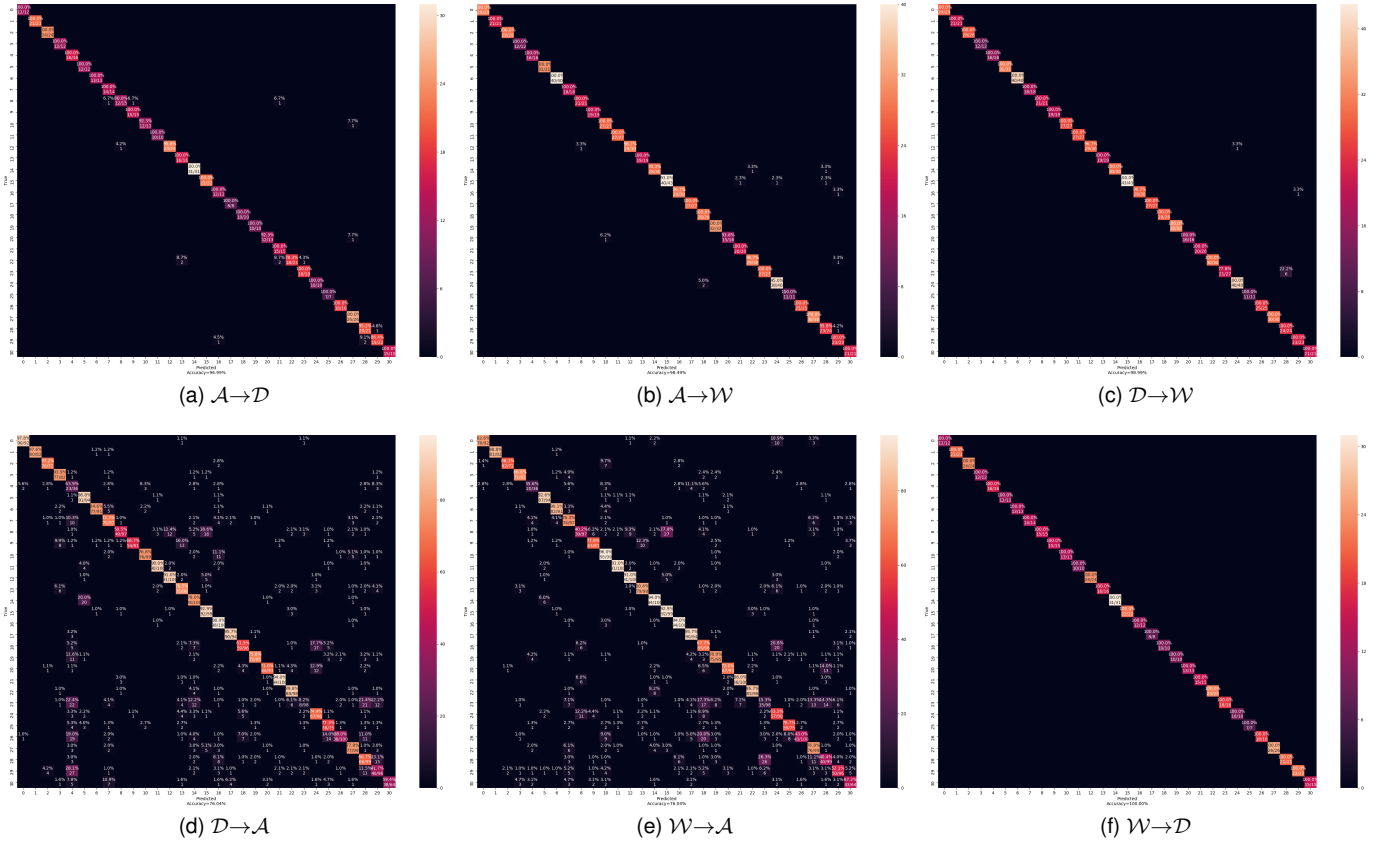


Fig. 8. Confusion matrices corresponding to the target domain accuracy of CUDA in Table 2. The confusion matrices with real-world domains, \mathcal{D} and \mathcal{W} , as the target domain indicates lower complexity involved in real-world target domains. The confusion matrices with synthetic domain \mathcal{A} as the target domain indicates higher complexity involved in synthetic target domain. (Best viewed in color.)

TABLE 2

Target domain accuracy (%) on high resolution Office-31 [39] dataset containing three domains. CUDA corresponds to our best results obtained with best hyper-parameter settings. $ss=\mathcal{BL}_1$: source supervised (2), tu : target unsupervised (5), su : source unsupervised (5), sa : source adversarial regularization (9), and ta : target adversarial regularization (9) represents different training configurations.

Method	$\mathcal{A} \rightarrow \mathcal{D}$	$\mathcal{A} \rightarrow \mathcal{W}$	$\mathcal{D} \rightarrow \mathcal{A}$	$\mathcal{D} \rightarrow \mathcal{W}$	$\mathcal{W} \rightarrow \mathcal{A}$	$\mathcal{W} \rightarrow \mathcal{D}$	Mean
DAN [1]	78.6	80.5	63.6	97.1	62.8	99.6	80.3
RIN [2]	77.5	84.5	66.2	96.8	64.8	99.4	81.5
JAN [3]	84.7	85.4	68.6	97.4	70.0	99.8	84.3
Rozantsev et. al. [9]	75.5	75.8	55.7	96.7	57.6	99.6	76.8
RevGrad [17]	79.7	82.0	68.2	96.9	67.4	99.1	82.2
ADDA [19]	77.8	86.2	69.5	96.2	68.9	98.4	82.8
GTA [20]	87.7	89.5	72.8	97.9	71.4	99.8	86.5
CDAN [25]	92.9	94.1	71.0	98.6	69.3	100.0	87.6
ATM [33]	96.4	95.7	74.1	99.3	73.5	100.0	89.8
CADA-P [34]	95.6	97.0	71.5	99.3	73.1	100.0	89.5
PFAN [35]	76.3	83.0	63.3	99.0	60.8	99.9	80.4
DICE [29]	68.5	72.5	58.1	97.2	60.3	100.0	76.1
CUDA (Ours)	97.0	98.5	76.0	99.1	76.0	100.0	91.1
$ss=\mathcal{BL}_1$ (Ours) (fine-tune ResNet-50)	41.0	38.7	23.2	80.6	25.6	94.2	50.6
$ss=\mathcal{BL}_1$ (Ours) (fixed ResNet-50)	82.0	77.9	68.4	97.2	67.1	100.0	82.1
$ss+tu$ (Ours) (fixed ResNet-50)	95.0	93.8	71.5	98.9	73.3	99.4	88.7
$ss+tu+su$ (Ours) (fixed ResNet-50)	96.0	95.6	69.5	99.1	70.7	100.0	88.5
$ss+tu+su+ta$ (Ours) (fixed ResNet-50)	92.8	91.6	72.5	98.4	72.8	99.8	88.0
$ss+tu+su+ta+sa$ (Ours) (fixed ResNet-50)	91.8	95.6	73.2	98.0	74.7	100.0	88.9
$ss=\mathcal{BL}_1$ (Ours) (fixed ResNet-152)	84.9	82.8	70.3	98.2	71.1	100.0	84.6
$ss+tu$ (Ours) (fixed ResNet-152)	97.0	94.3	73.9	99.0	75.5	100.0	90.0
$ss+tu+su$ (Ours) (fixed ResNet-152)	95.6	95.6	73.8	98.7	74.3	100.0	89.7
$ss+tu+su+ta$ (Ours) (fixed ResNet-152)	97.0	97.4	76.0	98.6	75.1	99.8	90.7
$ss+tu+su+ta+sa$ (Ours) (fixed ResNet-152)	95.4	98.5	75.0	98.9	76.0	100.0	90.6

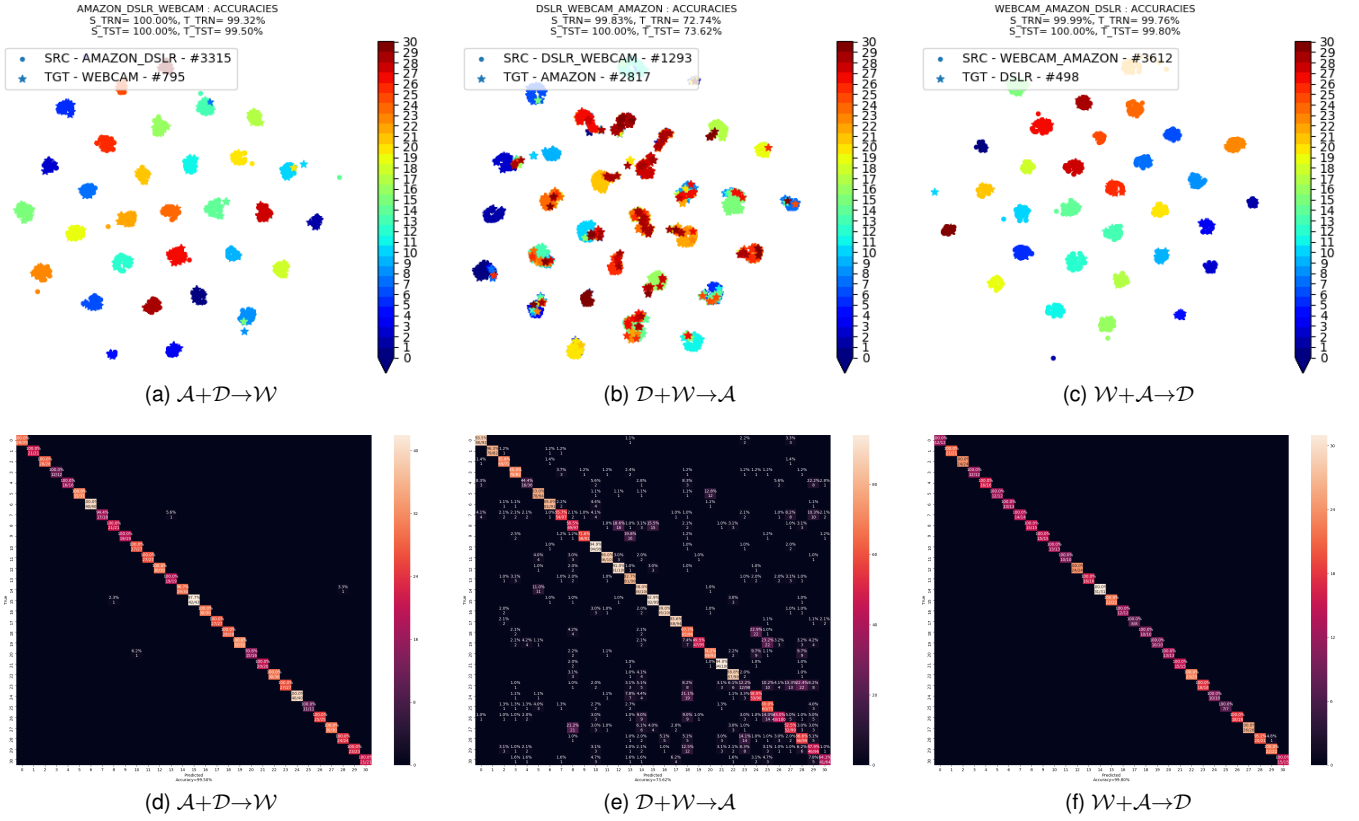


Fig. 9. Top Row: t-SNE [71] plots for embeddings from the output of contradistinguisher corresponding to the samples from Office-31 [39] dataset in high resolution visual tasks after applying softmax trained with CUDA with ResNet-50 [67] as the encoder in a **multi-source domain adaptation** setting. Bottom Row: Confusion matrices of target domain corresponding to respective t-SNE [71] plots in top row as indicated in Table 3. (Best viewed in color.)

TABLE 3

Target domain accuracy (%) on high resolution Office-31 [39] dataset under **multi-source domain adaptation** setting by combining two domains into a single source domain and the remaining domain as the target domain with ResNet-50 [67] as encoder. CUDA corresponds to our best results obtained with best hyper-parameter settings. $ss=\mathcal{BL}_1$: source supervised (2), tu : target unsupervised (5), su : source unsupervised (5), sa : source adversarial regularization (9), and ta : target adversarial regularization (9) represents different training configurations.

Setting	Method	$A+D \rightarrow W$	$D+W \rightarrow A$	$W+A \rightarrow D$	Mean
Best single source	DAN [1]	97.1	63.6	99.6	86.8
	RTN [2]	96.8	66.2	99.4	87.5
	JAN [3]	97.4	70.0	99.8	89.1
	Rozantsev et. al. [9]	96.7	57.6	99.6	84.6
	mDA-layer [10]	94.5	64.9	94.9	84.8
	RevGrad [17]	96.9	68.2	99.1	88.1
	ADDA [19]	96.2	69.5	98.4	88.0
	GTA [20]	97.9	72.8	99.8	90.2
	CDAN [25]	98.6	71.0	100.0	89.8
	DICE [29]	97.2	60.3	100.0	85.8
Multi-source	CUDA (Ours)	99.1	74.7	100.0	91.3
	DAN [1]	95.2	53.4	98.8	82.5
	mDA-layer [10]	94.6	62.6	93.7	83.6
	DIAL [13]	94.3	62.5	93.8	83.5
	RevGrad [17]	96.2	54.6	98.8	83.2
	DCTN [30]	96.9	54.9	99.6	83.8
	SGF [51]	52.0	28.0	39.0	39.7
	sFRAME [52]	52.2	32.1	54.5	46.3
	CUDA (Ours)	99.5	73.6	99.8	91.0
	$ss=\mathcal{BL}_1$ (Ours)	95.6	68.1	99.2	87.6
	$ss+tu$ (Ours)	99.4	72.1	99.8	90.4
	$ss+tu+su$ (Ours)	98.9	70.3	99.4	89.5
	$ss+tu+su+ta$ (Ours)	99.5	73.3	99.6	90.8
	$ss+tu+su+ta+sa$ (Ours)	99.4	73.6	99.2	90.7

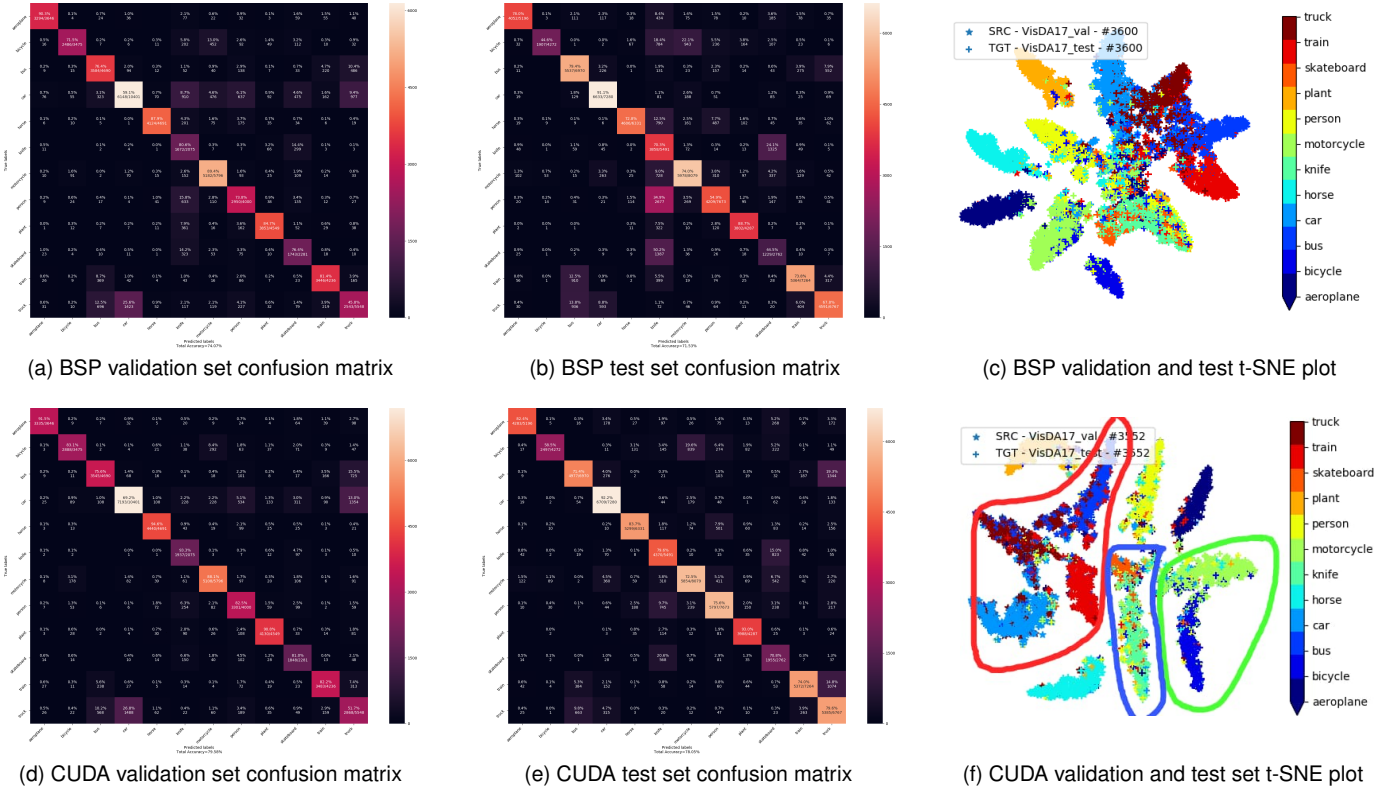


Fig. 10. Row 1: Best results reproduced from BSP. Row 2: Best results reproduced from CUDA. One-to-one comparison of the plots from BSP and CUDA clearly indicates that CUDA outperforms the current state-of-the-art by huge margins. The t-SNE plots of CUDA shows the clear clustering of all the twelve classes of VisDA-2017 distinctively compared to the t-SNE plots of BSP. The t-SNE plots of CUDA represents some important visual semantics of the image embeddings obtained from contradistinguisher in the following manner. (i) The vehicular classes such as ‘bus’, ‘car’, ‘train’, and ‘truck’ can be seen clustered closely as semantically these classes are similar to each other (region bounded in red). (ii) The two wheeler classes such as ‘bicycle’, and ‘motorcycle’ are clustered closely as these are semantically similar to each other in comparison to vehicular classes which are clustered exactly opposite (region bounded in green). (iii) Irrespective of the approach used, there is always a confusion between ‘knife’, and ‘skateboard’ classes. This confusion between ‘knife’, and ‘skateboard’ classes represented in the confusion matrices, which is also clearly seen in the t-SNE plots as well, can be attributed to the nature of images of these classes in the dataset on close observation (region bounded in blue). (iv) The remaining classes such as ‘aeroplane’, ‘horse’, ‘person’, and ‘plant’ can be seen clustered independently and distinctively as these classes have almost no visual semantic similarities to one another. (Best viewed in color.)

TABLE 4

Results on VisDA-2017 dataset reproduced from the current state-of-the-art method BSP and our proposed method CUDA reported on both the validation set and test set. We report all the evaluation metric such precision, recall and accuracy unlike BSP where the recall scores are mistakenly reported as accuracy. All the results are reported from the respective confusion matrices shown in Fig 10.

Data-split	Metric (%)	Method	Aeroplane	Bicycle	Bus	Car	Horse	Knife	Motorcycle	Person	Plant	Skateboard	Train	Truck	Mean
Validation	Precision	BSP [31]	93.79	91.40	71.03	78.36	94.98	35.25	78.90	63.12	91.37	55.28	82.16	58.15	74.48
		CUDA	96.33	87.04	79.20	80.68	92.25	67.66	86.74	70.28	91.57	67.37	87.36	50.18	79.72
	Recall	BSP [31]	90.35	71.54	76.42	59.11	87.91	80.58	89.41	73.75	84.70	76.41	81.35	45.84	76.45
		CUDA	91.47	83.11	75.59	69.16	94.65	93.35	88.13	82.52	90.79	81.02	82.22	51.69	81.97
	Accuracy	TPN [14]	93.70	85.10	69.20	81.60	93.50	61.90	89.30	81.40	93.50	81.60	84.50	49.90	80.40
		BSP [31]	98.97	97.79	95.36	89.26	98.58	93.73	96.39	94.99	98.09	96.48	97.22	91.27	95.68
Test	Precision	CUDA	99.21	98.16	96.25	91.10	98.87	98.08	97.35	96.22	98.56	97.60	97.73	90.02	96.60
		BSP [31]	91.76	95.83	71.50	83.08	94.87	33.08	76.45	72.25	87.38	34.54	83.36	80.12	75.35
	Recall	CUDA	93.31	94.44	81.28	82.26	91.77	66.12	80.43	77.37	88.48	45.19	89.43	60.74	79.24
		BSP [31]	77.98	44.64	79.44	91.11	72.75	70.26	73.99	54.85	88.69	44.50	73.84	67.84	69.99
	Accuracy	CUDA	82.41	58.45	71.41	92.16	83.70	79.58	72.46	75.55	93.03	70.78	73.95	79.58	77.75
		BSP [31]	97.92	96.62	94.97	97.24	97.27	86.96	94.55	92.98	98.57	94.66	95.89	95.42	95.25
		CUDA	98.31	97.34	95.66	97.21	97.92	95.36	94.96	95.06	98.87	95.61	96.51	93.28	96.34

main adaptation task, (ii) Figs 7a and 7b indicate moderately high accuracies because of synthetic to real-world domain adaptation task, and (iii) Figs 7d and 7e indicate lowest accuracies among all the six tasks because of real-world to synthetic domain adaptation task. Fig 8 reiterates the above

observations involving synthetic and real-world domains. In Figs 8d and 8e, we can observe the highest misclassification as the domain adaptation task involves in the direction from real-world to synthetic domain, which is a relatively complex task as also seen consistently in other baseline

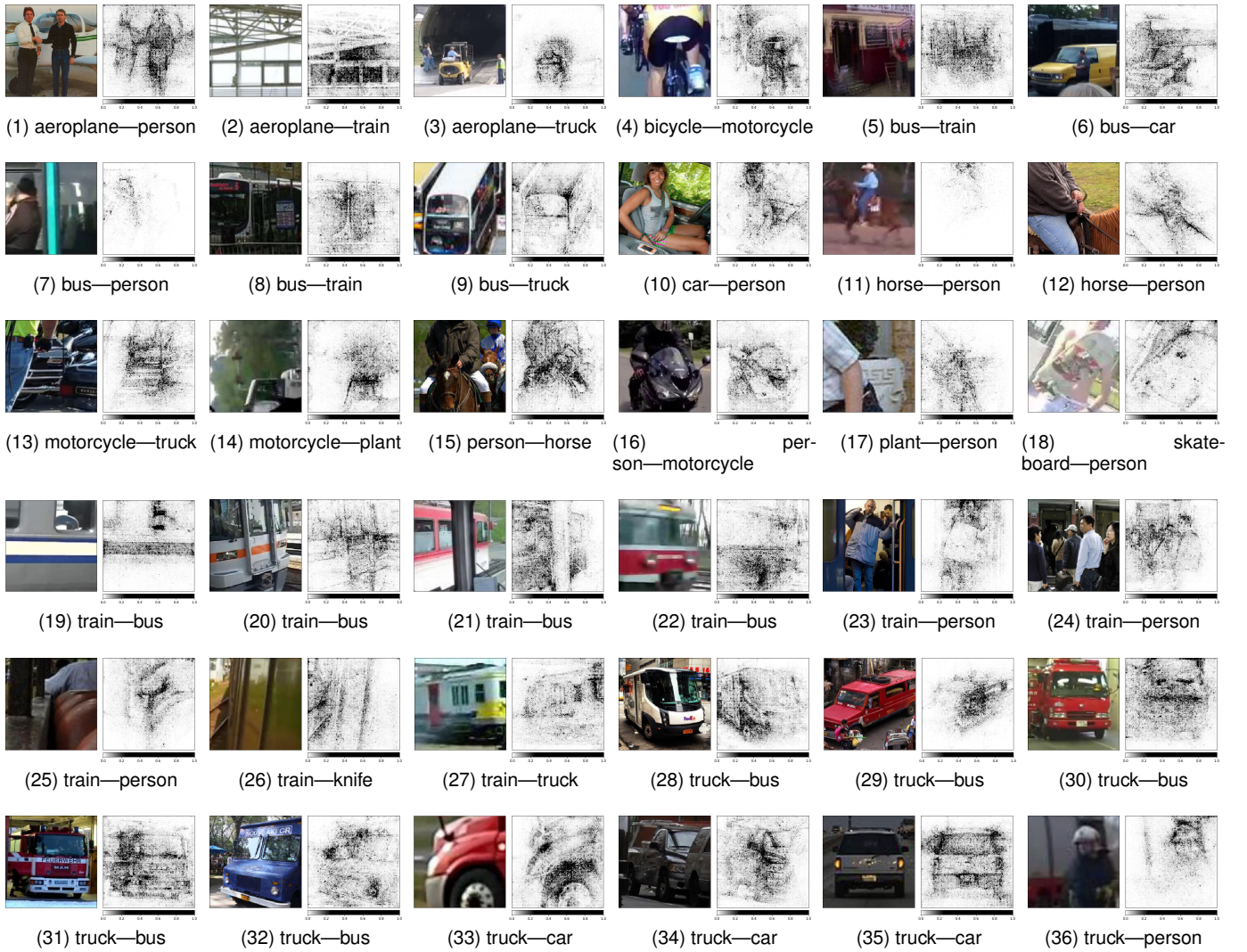


Fig. 11. We indicate few samples that are misclassified by the contradistinguisher in the following subcaption format ‘original_label—predicted_label’. In most cases, the original ground truth labels are dubious and the predicted labels make more sense realistically. The visualization of the features responsible for the respective predicted outcome indicates the shape bias as mostly the features are detected as edges corresponding to the shape of the object in the image. This shows the importance of shape bias to achieve high performance in transfer learning and domain adaptation tasks.

TABLE 5

Total classification accuracy (%) on VisDA-2017 dataset reported on both the validation set and test set. The results from JAN, GTA, CDAN and TransNorm are reported from TransNorm [32]. The results from BSP and CUDA reported from the confusion matrices in Fig 10.

Method	Data-split	
	Validation	Test
JAN [3]	61.6	-
GTA [20]	69.5	-
CDAN [25]	70.0	-
TransNorm [32]	71.4	-
BSP [31]	74.1	71.5
CUDA [38]	79.6	78.1

domain adaptation methods.

4.4.2 Office-31 Dataset Multi-Source Domain Adaptation Results

We also extend the experiments to multi-source domain adaptation on the Office-31 [39] dataset. In Table 3, we can clearly observe that in $\mathcal{A}+\mathcal{D}\rightarrow\mathcal{W}$ task, multi-source domain adaptation provides better results than their respective best single source domain adaptation experiments. However in case of $\mathcal{D}+\mathcal{W}\rightarrow\mathcal{A}$ and $\mathcal{W}+\mathcal{A}\rightarrow\mathcal{D}$, the multi-source domain adaptation improves over \mathcal{BC}_1 , it underperforms compared to best single source domain adaptation task. This can be attributed to the fact that model is overfitting on the source domains resulting in a negative transfer. This behavior of negative transfer is also prevalent in other multi-source domain adaptation approaches since all the other multi-source domain adaptation methods also underperform when compared to their best single source domain adaptation results as reported in Table 3. Figs 9a-9c indicates t-SNE [71] plots for embeddings from the output of contradistinguisher corresponding to the samples from

Office-31 [39] dataset after applying softmax trained with CUDA with ResNet-50 [67] as the encoder in a **multi-source domain adaptation** setting. We can observe the best results when the target domain is one of the real-world domain, i.e., \mathcal{D} and \mathcal{W} . It was consistently observed that domain adaptation tasks with synthetic domain \mathcal{A} as the target domain to be the most complex tasks of all the domain adaptation tasks across all the domain adaptation methods. Figs 9d-9f indicates the confusion matrix of target domain corresponding to their respective t-SNE [71] plots in Figs 9a-9c respectively.

4.4.3 VisDA-2017 Dataset Domain Adaptation Results

In Fig 10, we report the results reproduced from the current state-of-the-art unsupervised domain adaptation approach BSP [31] in comparison with our approach CUDA on both the pre-defined validation split (seen target domain training set) and testing split (unseen target domain testing set) of the VisDA-2017 dataset. In Table 4 we compare the per-class precision, recall and accuracies on both the pre-defined validation set and test set of VisDA-2017 dataset against the results reproduced from BSP. In Table 5 we compare the total classification accuracies on both the pre-defined validation set and test set of VisDA-2017 dataset against different benchmark methods. The results in Tables 4 and 5 indicate the superior performance of proposed method CUDA over BSP on both the pre-defined validation set and test set of VisDA-2017 dataset. Even though the validation set and test set belong to real-world domain, there is an inherent domain shift between them as both the datasplits are collected from two different datasets, i.e. MS COCO [69] and YouTube Bounding Boxes [70] respectively. Results from CUDA indicate a better generalization to real-world domain as the scores in validation and test sets are closer compared to other approaches on VisDA-2017 dataset. We can also observe that the t-SNE plot of CUDA in Fig 10f clearly shows the visual semantics captured between the classes of images in the VisDA-2017 dataset.

Apart from setting CUDA as the solid baseline for VisDA-2017, we further carefully investigated the reasons for misclassification from the contradistinguisher to check if we can further improve the results. In most misclassified cases, we have observed that the labels predicted by CUDA appears to be correct in comparison to the ground truth label of the dataset. In Fig 11, we present some of these instances from the off diagonal elements in the confusion matrices where the predicted label is more close to the real label than the ground truth. This misclassification is observed due to the fact that some of the images consists of objects belonging to more than one of the twelve classes. In such a case, the predicted label from the model cannot be considered as a wrong label as it contains the object of the predicted label in the image. We believe that this is the one of the reasons for the overall low performance apart from the complexity of the VisDA-2017 dataset compared to other visual datasets.

4.4.4 Analysis of Contradistinguisher Interpretability

Here, we analyse the nature of the feature representations learnt by contradistinguisher. In order to visualize the features, we use Captum², an open source, extensible library

for model interpretability built on PyTorch³ [73]. In terms of high level features in a given image, one can imagine features such as shape, color, texture, size etc. to be the features that help in predicting the classifier outcome. Out of all these features, the most natural and basic feature influencing the outcome is observed to be the shapes of the objects. Extensive research materials in psychology such as [74], [75], [76], [77], [78] have indicated that human babies and adults tend to utilize shapes than color/material/texture to assign a word label to the given object. This particular phenomena is widely termed as ‘shape bias’ in the literature. However recently, it was shown that the ImageNet pre-trained models posses a texture bias over shape bias [43]. To improve the shape bias, [43] propose a new modified dataset called ‘Stylized-ImageNet’ to overcome the texture bias. By increasing the shape bias, [43] demonstrated an improved performance and robustness. Since we use the ImageNet pre-trained ResNet-101 as a feature extractor, it is necessary to understand the nature of extracted features from the input images.

Unlike ‘Stylized-ImageNet’, in domain adaptation tasks, one cannot always expect to get such curated dataset with ground truth labels on the target domain for each task. Instead, it might be easy and desirable to change the loss function that learns the features during the training with the same dataset and learn shape features. Surprisingly, in our investigations, we find that the features learnt using our unsupervised loss, i.e. contradistinguishing loss indicate the high level features or the saliency maps [79] representing the shape of the object in the image. The contradistinguishing loss is formulated and optimized in such a way that the features extracted are most unique and contrastive for a given image in comparison to other images in the dataset. This consequently is observed as the features corresponding to shapes in the form of silhouette in the feature visualizations in Fig 11 as each objects posses unique shape as their most contradistinguishing character, i.e. the character which is most discriminative and unique to the given image. In particular, due the nature of VisDA-2017 dataset, the only positive transfer learning can be through transferring the shape features learnt from source domain because the grayscale images from the synthetic source domain lack either colors or textures. Any transfer of colors/textures features would lead to negative transfer from source domain to target domain resulting in a reduced generalization performance on the target domain.

5 CONCLUDING REMARKS

In this paper, we have proposed a direct approach for the problem of unsupervised domain adaptation that is different from the standard distribution alignment approaches. In our approach, we jointly learn a Contradistinguisher on the source and target domain distribution in the same input-label feature space using contradistinguishing loss for unsupervised target domain to identify contrastive features. We have shown that the contrastive learning overcomes the need and drawbacks of domain alignment, especially in tasks where domain shift is very high (e.g., language

2. <https://captum.ai/>

3. <https://pytorch.org/>

domains) and data augmentation techniques cannot be applied. Due to the inclusion of prior enforcing in the contradistinguishing loss, the proposed unsupervised domain adaptation method CUDA could incorporate any known target domain prior to overcome the drawbacks of skewness in the target domain, thereby resulting in a skew-robust model. We validated the efficacy of CUDA by experimenting on the synthetically created toy-dataset. We further demonstrated the simplicity and effectiveness of our proposed method by performing multi-source domain adaptation and consistently outperformed other multi-source domain adaptation approaches.

We have also tested the proposed method CUDA on the recent benchmark visual domain adaptation datasets such as Office-31 and VisDA-2017 classification datasets and demonstrated above/on-par results with the state-of-the-art approaches. We further analysed the nature of the feature representation learnt using contradistinguishing loss to identify the features related to the shapes that influence the predicted outcome. As the features related to shapes are learnt, we demonstrated that it helps improve the performance and robustness of the trained model as the model is not biased to colors/textures in the images. We concluded that learning and improving shape bias is the key to achieving ideal transfer learning and domain adaptation. With this work, we have taken the first step towards motivating the advantage and the need for unsupervised learning based domain adaptation approaches to improve the shape bias compared to widely existing domain alignment based approaches.

ACKNOWLEDGMENTS

The authors would like to thank Ministry of Human Resource Development (MHRD), Government of India, for their generous funding towards this work through UAY Project: IISc 001. The authors thank Shubham Gupta for providing valuable suggestions on the first draft of this manuscript. The authors would also like to thank anonymous reviewers for providing their valuable feedback that helped in improving the manuscript.

REFERENCES

- [1] M. Long, Y. Cao, J. Wang, and M. I. Jordan, "Learning transferable features with deep adaptation networks," in *ICML*, 2015.
- [2] M. Long, H. Zhu, J. Wang, and M. I. Jordan, "Unsupervised domain adaptation with residual transfer networks," in *NIPS*, 2016.
- [3] —, "Deep transfer learning with joint adaptation networks," in *ICML*, 2017.
- [4] P. Häusser, T. Frerix, A. Mordvintsev, and D. Cremers, "Associative domain adaptation," in *ICCV*, 2017.
- [5] K. Saito, K. Watanabe, Y. Ushiku, and T. Harada, "Maximum classifier discrepancy for unsupervised domain adaptation," in *CVPR*, 2018.
- [6] G. French, M. Mackiewicz, and M. Fisher, "Self-ensembling for visual domain adaptation," in *ICLR*, 2018.
- [7] C. Louizos, K. Swersky, Y. Li, M. Welling, and R. S. Zemel, "The variational fair autoencoder," in *ICLR*, 2016.
- [8] W. Zellinger, T. Grubinger, E. Lughofer, T. Natschlager, and S. Saminger-Platz, "Central moment discrepancy (CMD) for domain-invariant representation learning," in *ICLR*, 2017.
- [9] A. Rozantsev, M. Salzmann, and P. Fua, "Beyond sharing weights for deep domain adaptation," *IEEE Transactions on Pattern Analysis and Machine Intelligence (TPAMI)*, 2019.
- [10] M. Mancini, L. Porzi, S. Rota Bulò, B. Caputo, and E. Ricci, "Inferring latent domains for unsupervised deep domain adaptation," *IEEE Transactions on Pattern Analysis and Machine Intelligence (TPAMI)*, 2019.
- [11] —, "Boosting domain adaptation by discovering latent domains," in *CVPR*, 2018.
- [12] F. M. Carlucci, L. Porzi, B. Caputo, E. Ricci, and S. R. Bulò, "Autodial: Automatic domain alignment layers," in *ICCV*, 2017.
- [13] —, "Just dial: Domain alignment layers for unsupervised domain adaptation," in *ICIAP*, 2017.
- [14] Y. Pan, T. Yao, Y. Li, Y. Wang, C. Ngo, and T. Mei, "Transferrable Prototypical Networks for Unsupervised Domain Adaptation," in *CVPR*, 2019.
- [15] M. Ghifary, W. B. Kleijn, M. Zhang, D. Balduzzi, and W. Li, "Deep reconstruction-classification networks for unsupervised domain adaptation," in *ECCV*, 2016.
- [16] K. Bousmalis, G. Trigeorgis, N. Silberman, D. Krishnan, and D. Erhan, "Domain separation networks," in *NIPS*, 2016.
- [17] Y. Ganin and V. Lempitsky, "Unsupervised domain adaptation by backpropagation," in *ICML*, 2015.
- [18] M. Liu and O. Tuzel, "Coupled generative adversarial networks," in *NIPS*, 2016.
- [19] E. Tzeng, J. Hoffman, K. Saenko, and T. Darrell, "Adversarial discriminative domain adaptation," in *CVPR*, 2017.
- [20] S. Sankaranarayanan, Y. Balaji, C. D. Castillo, and R. Chellappa, "Generate to adapt: Aligning domains using generative adversarial networks," in *CVPR*, 2018.
- [21] Y. C. Liu, Y. Y. Yeh, T. C. Fu, S. D. Wang, W. C. Chiu, and Y. C. F. Wang, "Detach and adapt: Learning cross-domain disentangled deep representation," in *CVPR*, 2018.
- [22] P. Russo, F. M. Carlucci, T. Tommasi, and B. Caputo, "From source to target and back: Symmetric bi-directional adaptive gan," in *CVPR*, 2018.
- [23] J. Hoffman, E. Tzeng, T. Park, J. Zhu, P. Isola, K. Saenko, A. Efros, and T. Darrell, "CyCADA: Cycle-consistent adversarial domain adaptation," in *ICML*, 2018.
- [24] S. Xie, Z. Zheng, L. Chen, and C. Chen, "Learning semantic representations for unsupervised domain adaptation," in *ICML*, 2018.
- [25] M. Long, Z. Cao, J. Wang, and M. I. Jordan, "Conditional adversarial domain adaptation," in *NIPS*, 2018.
- [26] C. Chen, Z. Chen, B. Jiang, and X. Jin, "Joint domain alignment and discriminative feature learning for unsupervised deep domain adaptation," in *AAAI*, 2019.
- [27] R. Shu, H. Bui, H. Narui, and S. Ermon, "A DIRT-t approach to unsupervised domain adaptation," in *ICLR*, 2018.
- [28] E. Hosseini-Asl, Y. Zhou, C. Xiong, and R. Socher, "Augmented cyclic adversarial learning for low resource domain adaptation," in *ICLR*, 2019.
- [29] J. Liang, R. He, Z. Sun, and T. Tan, "Aggregating randomized clustering-promoting invariant projections for domain adaptation," *IEEE Transactions on Pattern Analysis and Machine Intelligence (TPAMI)*, 2018.
- [30] R. Xu, Z. Chen, W. Zuo, J. Yan, and L. Lin, "Deep cocktail network: Multi-source unsupervised domain adaptation with category shift," in *CVPR*, 2018.
- [31] X. Chen, S. Wang, M. Long, and J. Wang, "Transferability vs. discriminability: Batch spectral penalization for adversarial domain adaptation," in *ICML*, 2019.
- [32] X. Wang, Y. Jin, M. Long, J. Wang, and M. I. Jordan, "Transferable Normalization: Towards Improving Transferability of Deep Neural Networks," in *NIPS*, 2019.
- [33] J. Li, E. Chen, Z. Ding, L. Zhu, K. Lu, and H. T. Shen, "Maximum Density Divergence for Domain Adaptation," *IEEE Transactions on Pattern Analysis and Machine Intelligence (TPAMI)*, 2020.
- [34] V. K. Kurmi, S. Kumar, and V. P. Namboodiri, "Attending to Discriminative Certainty for Domain Adaptation," in *CVPR*, 2019.
- [35] C. Chen, W. Xie, W. Huang, Y. Rong, X. Ding, Y. Huang, T. Xu, and J. Huang, "Progressive Feature Alignment for Unsupervised Domain Adaptation," in *CVPR*, 2019.
- [36] V. N. Vapnik, "An overview of statistical learning theory," *IEEE transactions on neural networks*, 1999.
- [37] V. Vapnik, *The nature of statistical learning theory*. Springer Science & Business Media, 2013.
- [38] S. Balgi and A. Dukkupati, "Cuda: Contradistinguisher for unsupervised domain adaptation," in *ICDM*, 2019.

- [39] K. Saenko, B. Kulis, M. Fritz, and T. Darrell, "Adapting visual category models to new domains," in *ECCV*, 2010.
- [40] X. Peng, B. Usman, N. Kaushik, J. Hoffman, D. Wang, and K. Saenko, "VisDA: The Visual Domain Adaptation Challenge," *CoRR*, 2017.
- [41] G. Pandey and A. Dukkipati, "Unsupervised feature learning with discriminative encoder," in *ICDM*, 2017.
- [42] F. Pedregosa, G. Varoquaux, A. Gramfort, V. Michel, B. Thirion, O. Grisel, M. Blondel, P. Prettenhofer, R. Weiss, V. Dubourg *et al.*, "Scikit-learn: Machine learning in python," *Journal of Machine Learning Research (JMLR)*, 2011.
- [43] R. Geirhos, P. Rubisch, C. Michaelis, M. Bethge, F. A. Wichmann, and W. Brendel, "ImageNet-trained CNNs are biased towards texture; increasing shape bias improves accuracy and robustness," in *ICLR*, 2019.
- [44] A. Gretton, K. Fukumizu, Z. Harchaoui, and B. K. Sriperumbudur, "A fast, consistent kernel two-sample test," in *NIPS*, 2009.
- [45] A. Gretton, K. M. Borgwardt, M. J. Rasch, B. Schölkopf, and A. Smola, "A kernel two-sample test," *Journal of Machine Learning Research (JMLR)*, 2012.
- [46] D. Sejdinovic, B. Sriperumbudur, A. Gretton, K. Fukumizu *et al.*, "Equivalence of distance-based and rkhs-based statistics in hypothesis testing," *The Annals of Statistics*, 2013.
- [47] A. Tarvainen and H. Valpola, "Mean teachers are better role models: Weight-averaged consistency targets improve semi-supervised deep learning results," in *NIPS*, 2017.
- [48] S. Laine and T. Aila, "Temporal ensembling for semi-supervised learning," in *ICLR*, 2017.
- [49] D. P. Kingma and M. Welling, "Auto-encoding variational bayes," in *ICLR*, 2014.
- [50] S. Ioffe and C. Szegedy, "Batch normalization: Accelerating deep network training by reducing internal covariate shift," in *ICML*, 2015.
- [51] R. Gopalan, R. Li, and R. Chellappa, "Domain adaptation for object recognition: An unsupervised approach," in *ICCV*, 2011.
- [52] J. Xie, W. Hu, S.-C. Zhu, and Y. N. Wu, "Learning sparse frame models for natural image patterns," *International Journal of Computer Vision (IJCV)*, 2015.
- [53] Y. Ganin, E. Ustinova, H. Ajakan, P. Germain, H. Larochelle, F. Laviolette, M. Marchand, and V. Lempitsky, "Domain-adversarial training of neural networks," *Journal of Machine Learning Research (JMLR)*, 2016.
- [54] I. J. Goodfellow, J. Pouget-Abadie, M. Mirza, B. Xu, D. Warde-Farley, S. Ozair, A. Courville, and Y. Bengio, "Generative adversarial nets," in *NIPS*, 2014.
- [55] K. Saito, Y. Ushiku, and T. Harada, "Asymmetric tri-training for unsupervised domain adaptation," in *ICML*, 2017.
- [56] S. Ruder and B. Plank, "Strong baselines for neural semi-supervised learning under domain shift," in *ACL*, 2018.
- [57] A. P. Dempster, N. M. Laird, and D. B. Rubin, "Maximum likelihood from incomplete data via the em algorithm," *Journal of the Royal Statistical Society: Series B (Methodological)*, 1977.
- [58] D.-H. Lee, "Pseudo-label: The simple and efficient semi-supervised learning method for deep neural networks," *ICML Workshops (WREPL)*, 2013.
- [59] Y. Grandvalet and Y. Bengio, "Semi-supervised learning by entropy minimization," in *NIPS*, 2005.
- [60] C. L. Li, W. C. Chang, Y. Cheng, Y. Yang, and B. Póczos, "MMD-GAN: Towards deeper understanding of moment matching network," in *NIPS*, 2017.
- [61] Y. LeCun, B. Boser, J. S. Denker, D. Henderson, R. E. Howard, W. Hubbard, and L. D. Jackel, "Backpropagation applied to handwritten zip code recognition," *Neural Computation*, 1989.
- [62] Y. LeCun, L. Bottou, Y. Bengio, P. Haffner *et al.*, "Gradient-based learning applied to document recognition," *IEEE*, 1998.
- [63] Y. Netzer, T. Wang, A. Coates, A. Bissacco, B. Wu, and A. Y. Ng, "Reading digits in natural images with unsupervised feature learning," in *NIPS Workshop on Deep Learning and Unsupervised Feature Learning*, 2011.
- [64] A. Krizhevsky, "Learning multiple layers of features from tiny images," *Citeseer, Tech. Rep.*, 2009.
- [65] A. Coates, A. Ng, and H. Lee, "An analysis of single-layer networks in unsupervised feature learning," in *AISTATS*, 2011.
- [66] J. Stallkamp, M. Schlipsing, J. Salmen, and C. Igel, "The German traffic sign recognition benchmark: A multi-class classification competition," in *IJCNN*, 2011.
- [67] K. He, X. Zhang, S. Ren, and J. Sun, "Deep residual learning for image recognition," in *CVPR*, 2016.
- [68] J. Jacobsen, J. Behrmann, R. S. Zemel, and M. Bethge, "Excessive invariance causes adversarial vulnerability," in *ICLR*, 2019.
- [69] T. Lin, M. Maire, S. J. Belongie, J. Hays, P. Perona, D. Ramanan, P. Dollár, and C. L. Zitnick, "Microsoft COCO: Common Objects in Context," in *ECCV*, 2014.
- [70] E. Real, J. Shlens, S. Mazzocchi, X. Pan, and V. Vanhoucke, "YouTube-BoundingBoxes: A Large High-Precision Human-Annotated Data Set for Object Detection in Video," in *CVPR*, 2017.
- [71] L. van der Maaten and G. Hinton, "Visualizing data using t-SNE," *Journal of Machine Learning Research (JMLR)*, 2008.
- [72] Y. Zhang and B. D. Davison, "Impact of ImageNet Model Selection on Domain Adaptation," in *WACV Workshops*, 2020.
- [73] A. Paszke, S. Gross, S. Chintala, G. Chanan, E. Yang, Z. DeVito, Z. Lin, A. Desmaison, L. Antiga, and A. Lerer, "Automatic differentiation in PyTorch," *NIPS Workshops*, 2017.
- [74] B. Landau, L. B. Smith, and S. Jones, "Syntactic context and the shape bias in children's and adults' lexical learning," *Journal of Memory and Language*, 1992.
- [75] G. Diesendruck and P. Bloom, "How specific is the shape bias?" *Child development*, 2003.
- [76] E. R. Potrzeba, D. Fein, and L. Naigles, "Investigating the shape bias in typically developing children and children with autism spectrum disorders," *Frontiers in Psychology*, 2015.
- [77] S. Ritter, D. G. Barrett, A. Santoro, and M. M. Botvinick, "Cognitive psychology for deep neural networks: A shape bias case study," in *ICML*, 2017.
- [78] H. Hosseini, B. Xiao, M. Jaiswal, and R. Poovendran, "Assessing shape bias property of Convolutional Neural Networks," in *CVPR Workshops*, 2018.
- [79] K. Simonyan, A. Vedaldi, and A. Zisserman, "Deep Inside Convolutional Networks: Visualising Image Classification Models and Saliency Maps," in *ICLR Workshop*, 2014.



Sourabh Balgi received his B.E. degree in Electronics and Communication Engineering from Sri Jayachamarajendra College of Engineering, Mysore, India in 2013. He worked at Mercedes-Benz Research and Development India, Bangalore as a software engineer from 2013 to 2016. He received his M.Tech. degree in Artificial Intelligence from Indian Institute of Science (IISc), Bangalore, India in 2019. He is currently a Research Associate at the Statistics and Machine Learning Lab at the Department of Computer

Science and Automation, Indian Institute of Science (IISc), Bangalore, India, advised by Prof. Ambedkar Dukkipati. His research interests include unsupervised deep learning for computer vision, and machine learning with an emphasis on transfer learning, specifically domain adaptation and disentangled representation learning for domain adaptation and causal inference.



Ambedkar Dukkipati received his Ph.D. degree from the Department of Computer Science and Automation, Indian Institute of Science (IISc), Bangalore, India. He held a post-doctoral position at EURANDOM, Netherlands. Currently, he is an Associate Professor at the Department of Computer Science and Automation, IISc. He also heads the Statistics and Machine Learning group at the Department of Computer Science and Automation, IISc. His research interests include statistical network analysis, network representation learning, spectral graph methods, machine learning in low data regime, sequential decision-making under uncertainty and deep reinforcement learning.

representation learning, spectral graph methods, machine learning in low data regime, sequential decision-making under uncertainty and deep reinforcement learning.